

Improved estimate of global gross primary production for reproducing its long-term variation, 1982-2017

Yi Zheng¹, Ruoque Shen¹, Yawen Wang^{1,2}, Xiangqian Li¹, Shuguang Liu³, Shunlin Liang^{4,5}, Jing M. Chen^{6,7}, Weimin Ju^{7,8}, Li Zhang⁹, Wenping Yuan^{1,2*}

- 5 ¹School of Atmospheric Sciences, Sun Yat-sen University, Zhuhai 519082, Guangdong, China;
²Southern Laboratory of Ocean Science and Engineering (Guangdong, Zhuhai), Zhuhai 519000, Guangdong, China
³College of Life Science and Technology, Central South University of Forestry and Technology (CSUFT), Changsha, Hunan 410004, China
⁴Department of Geographical Sciences, University of Maryland, College Park, MD 20742 USA
10 ⁵School of Remote Sensing Information Engineering, Wuhan University, Wuhan 430072, Hubei, China
⁶Department of Geography, University of Toronto, Canada, M5G 3G3
⁷International Institute for Earth System Sciences, Nanjing University, Nanjing, China.
⁸Jiangsu Center for Collaborative Innovation in Geographical Information Resource Development and Application, Nanjing, China.
15 ⁹Key Laboratory of Digital Earth Science, Institute of Remote Sensing and Digital Earth, Chinese Academy of Sciences, Beijing 100094, China

Correspondence to: yuanwpcn@126.com (W. Yuan).

Abstract. Satellite-based models have been widely used to simulate vegetation gross primary production (GPP) at the site, regional, or global scales in recent years. However, accurately reproducing the interannual variations in GPP remains a major
20 challenge, and the long-term changes in GPP remain highly uncertain. In this study, we generated a long-term global GPP dataset at 0.05° latitude by 0.05° longitude and 8-day interval by revising a light use efficiency model (i.e. EC-LUE model). In the revised EC-LUE model, we integrated the regulations of several major environmental variables: atmospheric CO₂ concentration, radiation components, and atmospheric vapor pressure deficit (VPD). These environmental variables showed substantial long-term changes, which could greatly impact the global vegetation productivity. Eddy covariance (EC)
25 measurements at 95 towers from the FLUXNET2015 dataset, covering nine major ecosystem types around the globe, were used to calibrate and validate the model. In general, the revised EC-LUE model could effectively reproduce the spatial, seasonal, and annual variations in the tower estimated GPP at most sites. The revised EC-LUE model could explain 71% of the spatial variations in annual GPP over 95 sites. At more than 95% of the sites, the correlation coefficients (R^2) of seasonal changes between tower estimated and model simulated GPP are larger than 0.5. Particularly, the revised EC-LUE model improved the
30 model performance in reproducing the interannual variations in GPP, and the averaged R^2 between annual mean tower estimated and model simulated GPP is 0.62 over all 55 sites with observations longer than 5-years, which is significantly higher than those of original EC-LUE model ($R^2 = 0.36$) and other LUE models (R^2 ranged from 0.06 to 0.30 with an average value of 0.16). At the global scale, GPP derived from light use efficiency models, machine learning models, and processes-based biophysical models exist substantial differences in magnitude and interannual variations. The revised EC-LUE model
35 quantified the mean global GPP from 1982 to 2017 as 106.2 ± 2.9 Pg C yr⁻¹ with the trend 0.15 Pg C yr⁻¹. Sensitivity analysis

indicated that GPP simulated by the revised EC-LUE model was sensitive to atmospheric CO₂ concentration, VPD, and radiation. Over the period of 1982–2017, the CO₂ fertilization effect on the global GPP ($0.22 \pm 0.07 \text{ Pg C yr}^{-1}$) could be partly offset by increased VPD ($-0.17 \pm 0.06 \text{ Pg C yr}^{-1}$). The long-term changes in the environmental variables could be well reflected in global GPP. Overall, the revised EC-LUE model is able to provide a reliable long-term estimate of global GPP. The GPP dataset is available at <https://doi.org/10.6084/m9.figshare.8942336> (Zheng et al., 2019).

1 Introduction

Vegetation gross primary production (GPP) is the largest carbon flux component within terrestrial ecosystems and plays an essential role in regulating the global carbon cycle (Canadell et al., 2007; Zhao et al., 2010). As a primary variable of the terrestrial ecosystem cycle, GPP estimates will substantially determine other variables of the carbon cycle (Yuan et al., 2011).
45 Satellite-based GPP models have been developed based on the light use efficiency (LUE) principle (Monteith, 1972; Potter et al., 1993; Running et al., 2004; Xiao et al., 2005; Yuan et al., 2007). Thus far, LUE models have been a major tool for investigating the spatio-temporal changes in GPP and the environmental dominates, either independently or by combining with other ecosystem models (Keenan et al., 2016; Smith et al., 2016).

However, current LUE models exhibit poor performance in reproducing the interannual variations in GPP. A previous study
50 indicated that seven LUE models could only explain 6–36% of the interannual variations in GPP at 51 eddy covariance (EC) towers (Yuan et al., 2014). Similarly, a model comparison showed that none of the examined 16 processes-based biophysical models or the 3 remote sensing products (BESS, MODIS C5, and MODIS C5.1) could consistently reproduce the observed interannual variations in GPP at 11 forest sites in North America (Keenan et al., 2012). Seven LUE models simulated the long-term trends in global GPP varied from -0.15 to $1.09 \text{ Pg C yr}^{-1}$ over the period 2000–2010 (Cai et al., 2014). An important
55 reason for the poor performance in modeling the interannual variability is that the effect of environmental regulations on vegetation production is not completely integrated into the LUE models (Stocker et al., 2019). In particular, the long-term changes in several environmental variables are very important for accurately simulating the GPP series at the decadal scale.

Several environmental variables should be included in GPP models. Firstly, as we all know the rising atmospheric CO₂ concentration in the past few decades substantially stimulated global vegetation growth (Zhu et al., 2016; Liu et al., 2017).
60 Field experiments using greenhouses or open-top chambers showed that an increase of approximately 300 ppm in CO₂ concentration can increase the photosynthesis of C3 plants on the order of 60% (Norby et al., 1999). Free-air CO₂ enrichment (FACE) experiments generally confirmed the enhancement in net primary production (NPP) with the rising CO₂ concentration (Ainsworth and Long, 2005). For example, four FACE experiments indicated that the forest NPP consistently increased at the median of $23 \pm 2\%$ when the ambient CO₂ concentration was elevated to approximately 550 ppm (Norby et al., 2005).
65 According to observations, the atmospheric CO₂ concentration has risen by approximately 20% from 340 ppm (1982) to 410 ppm (2018) (<https://www.esrl.noaa.gov/>). However, the effects of CO₂ fertilization on GPP have not been integrated in most current satellite-based LUE models.

Secondly, solar radiation, or more specifically the photosynthetic active radiation (PAR) substantially influences the vegetation production of the terrestrial ecosystem (Alton et al., 2007; Kanniah et al., 2012; Krupkova et al., 2017). Study indicated that the solar radiation incident at the earth surface underwent significant decadal variations (Wild et al., 2005). A comprehensive analysis based on the datasets of worldwide distributed sites indicated significant decreases in solar radiation (2% per decade) from the late 1950s to 1990 in the regions of Asia, Europe, North America, and Africa (Gilgen et al., 1998). A later assessment by Wild et al. (2005) showed that the radiation increased at widespread locations since the mid-1980s.

However, not only the total amount of solar radiation or PAR incident at the earth surface but more importantly, their partitioning into direct and diffuse radiations, impact the vegetation productivity (Urban et al., 2007; Kanniah et al., 2012). Increased proportion of diffuse radiation enhances vegetation photosynthesis, because a higher blue/red light ratio within the diffuse radiation may lead to higher light use efficiency (Gu et al., 2002; Alton et al., 2007). For example, the sharply increased diffuse radiation induced by the 1991 Mount Pinatubo eruption enhanced the noontime vegetation productivity of a deciduous forest in the next 2 years (Gu et al. 2003). Besides volcanic aerosols, clouds could also reduce the total and direct radiation, while increase the proportion of diffuse radiation. Yuan et al. (2010) found that the higher LUE at European forests than North America was because of the higher ratio of cloudy days in Europe. Yuan et al. (2014) further proved that the significantly underestimated GPP during cloudy days by six LUE models was because the effects of diffuse radiation on LUE were neglected in these models.

Thirdly, atmospheric vapor pressure deficit (VPD) is another factor that should be included in GPP models. As an important driver of atmospheric water demand for plants, VPD influences terrestrial ecosystem function and photosynthesis (Rawson et al., 1977; Yuan, et al., 2019). Rising air temperature increases the saturated vapor pressure at a rate of $\sim 7\%/K$ according to the Clausius–Clapeyron relationship, and therefore, VPD will increase if the atmospheric water vapor content does not increase by exactly the same amount as the saturated vapor pressure. Numerous studies indicated significant changes in the relative humidity (ratio of actual water vapor pressure to saturated water vapor pressure) in both humid areas and continental areas located far from oceanic humidity (Van Wijngaarden and Vincent, 2004; Pierce et al., 2013). In particular, the global averaged land surface relative humidity decreased sharply after the late 1990s (Simmons et al. 2010; Willett et al. 2014) and the global averaged land surface VPD increased sharply after the late 1990s (Yuan, et al., 2019). The leaf and canopy photosynthetic rate declines when the atmospheric VPD increases due to stomatal closure (Fletcher et al., 2007). A recent study highlighted that increases in VPD rather than changes in precipitation would be a dominant influence on vegetation productivity (Konings et al., 2017). However, currently the influence of long-term VPD variations is not well expressed in many LUE models.

We have developed a LUE model, namely the EC-LUE model, by integrating remote sensing data and eddy covariance data to simulate daily GPP (Yuan et al., 2007; 2010). The model has been evaluated using the observations at EC towers located in Europe, North America, China, and East Asia, covering various ecosystem types (Yuan et al., 2007; 2010; Li et al., 2013). In this study, we revised the EC-LUE model by integrating the impacts of several environmental variables (i.e., atmospheric CO_2 concentration, radiation components, and atmospheric VPD) across a long-term temporal scale. Firstly, we evaluated the effectiveness of the revised EC-LUE model in determining the spatial, seasonal, and interannual variations in GPP from

multiple eddy covariance sites. Secondly, a global GPP dataset at 0.05° spatial resolution was generated based on the optimized model. Finally, we analyzed the contributions of the aforementioned environmental variables to the global GPP and discussed the spatial and interannual variations in GPP from different datasets.

105 **2 Data and Methods**

2.1 Data from the eddy covariance towers

The FLUXNET2015 dataset (<http://www.fluxdata.org>) includes over 200 variables of carbon fluxes, energy fluxes, and meteorological variables collected and processed at sites by the FLUXNET community. In our study, ninety-five EC sites in FLUXNET2015 dataset were utilized to optimize the parameters and evaluate the performance of the revised EC-LUE model, including nine major terrestrial ecosystem vegetation types (Table 1): evergreen broadleaf forests (EBF), evergreen needleleaf forests (ENF), deciduous broadleaf forests (DBF), mixed forests (MF), grasslands (GRA), savannas (SAV), shrubland (SHR), wetlands (WET), and croplands (CRO). More information about the characteristics of these sites can be referred to the FLUXNET website. For each site, the daily GPP, PAR, air temperature (T_a), and VPD were used in our study. The GPP variable (GPP_NT_VUT_REF) used in this study was estimated from night-time partitioning method. The corresponding net ecosystem exchange (NEE) was generated using variable friction velocity (USTAR) threshold for each year (VUT), in which 40 versions of NEE were created by using different percentiles of USTAR thresholds. The model efficiency between each version and the others 39 versions were calculated to test their similarities and the reference (REF) NEE was selected as the one with higher model efficiency sum (the most similar to the others 39). The daily meteorological 120 variables were gap-filled or downscaled from the ERA-interim reanalysis dataset in both space and time (Vuichard and Papale, 2015). The gap-filled technique of the carbon flux measurements and meteorological variables is the marginal distribution sampling (MDS) method described in Reichstein et al. (2005). In the FLUXNET dataset, there were quality flag ranged from 0 to 1 to indicate percentage of measured and good quality gap-filled data. For each variable, we used the daily/monthly values with more than 80% of good quality data (quality flag > 0.8). We aggregated the daily values to 8-day time step. And only the 8-day measurements with more than 5-day valid values were used.

125 <<Table 1>>

2.2 Data at the global scale

The global scale datasets used in this study are shown in Table 2. The meteorological reanalysis dataset was derived from the second Modern-Era Retrospective analysis for Research and Applications (MERRA-2) dataset. It was produced by NASA's Global Modeling and Assimilation Office that used an upgraded version of the GEOS-5 (Rienecker et al., 2011). It has been validated carefully using surface meteorological datasets and enhanced assimilation system to reduce the uncertainty in various meteorological variables globally. In our study, we obtained the daily mean air temperature (T_a , °C), mean dew point

temperature (T_d , °C), total direct PAR (PAR_{dr} , MJ m⁻² d⁻¹), and total diffuse PAR (PAR_{df} , MJ m⁻² d⁻¹) at 0.625° in longitude by 0.5° in latitude from 1982 to 2017. VPD was calculated from air temperature and dew point temperature:

$$SVP = 6.112 \times e^{\frac{17.67T_a}{T_a+243.5}} \quad (1)$$

$$135 \quad RH = e^{\frac{17.625T_d}{T_d+243.04} - \frac{17.625T_a}{T_a+243.04}} \quad (2)$$

$$VPD = SVP \times (1 - RH) \quad (3)$$

where SVP is the saturated vapor pressure (k Pa), and RH is the relative humidity. We aggregated the daily variables (air temperature, VPD, direct PAR, and diffuse PAR) to 8-day interval temporal resolution. And these variables were resampled to the spatial resolution of 0.05° latitude by 0.05° longitude using the bilinear interpolation method.

140 The 8-day Global LAnd Surface Satellite-leaf area index (GLASS LAI) dataset at 0.05° latitude by 0.05° longitude was adopted to indicate vegetation growth from 1982 to 2017. It was produced using the general regression neural networks (GRNNs) trained with the fused MOD15 LAI and CYCLOPES LAI and the preprocessed MODIS/AVHRR reflectance data over the BELMANIP sites (Xiao et al., 2016). Products validation and comparison showed that the GLASS LAI product was spatially complete and temporally continuous with lower uncertainty (Xu et al., 2018).

145 Additionally, the MCD12Q1 product with IGBP classification scheme was used as land cover map. The ISLSCP II C4 Vegetation Percentage map was used to separate the C3 and C4 crop. The NOAA's Earth System Research Laboratory (ESRL) CO₂ concentration dataset was used to express the CO₂ fertilization effect.

<<Table 2>>

2.3 The revised EC-LUE model

150 The terrestrial vegetation GPP can be expressed as follows in the revised EC-LUE model:

$$GPP = (\varepsilon_{msu} \times APAR_{su} + \varepsilon_{msh} \times APAR_{sh}) \times C_s \times \min(T_s, W_s) \quad (4)$$

where ε_{msu} is the maximum LUE of sunlit leaves; $APAR_{su}$ is the PAR absorbed by sunlit leaves; ε_{msh} is the maximum LUE of shaded leaves; $APAR_{sh}$ is the PAR absorbed by shaded leaves; C_s , T_s , and W_s represent the downward regulation scalars of atmospheric CO₂ concentration ([CO₂]), air temperature, and VPD on LUE ranging from 0 to 1; min represents the minimum value.

155 The effect of atmospheric CO₂ concentration on GPP is determined by the following equations (Farquhar et al., 1980; Collatz et al., 1991):

$$C_s = \frac{C_i - \varphi}{C_i + 2\varphi} \quad (5)$$

$$C_i = C_a \times \chi \quad (6)$$

160 where φ is the CO₂ compensation point in the absence of dark respiration (ppm); C_i is the leaf internal CO₂ concentration; C_a is the atmospheric CO₂ concentration; χ is the ratio of leaf internal to atmospheric CO₂ concentration which can be estimated as follows (Prentice et al., 2014; Keenan et al., 2016):

$$\chi = \frac{\varepsilon}{\varepsilon + \sqrt{VPD}} \quad (7)$$

$$\varepsilon = \sqrt{\frac{356.51K}{1.6\eta^*}} \quad (8)$$

165 where ε is a parameter related to the ‘carbon cost of water’, which means the sensitivity of VPD to χ ; K is the Michaelis–Menten coefficient of Rubisco; η^* is the viscosity of water relative to its value at 25 °C (Korson et al., 1969).

$$K = K_c \left(1 + \frac{P_o}{K_o}\right) \quad (9)$$

where P_o is the partial pressure of O_2 ; K_c and K_o are the Michaelis–Menten constants for CO_2 and O_2 (Keenan et al., 2016):

$$K_c = 39.97 \times e^{\frac{79.43 \times (T_a - 298.15)}{298.15 \times R \times T_a}} \quad (10)$$

$$170 \quad K_o = 27480 \times e^{\frac{36.38 \times (T_a - 298.15)}{298.15 \times R \times T_a}} \quad (11)$$

where T_a is air temperature (unit: K); R is the molar gas constant (8.314 J mol⁻¹ K⁻¹).

T_s and W_s can be expressed as follows:

$$T_s = \frac{(T_a - T_{min}) \times (T_a - T_{max})}{(T_a - T_{min}) \times (T_a - T_{max}) - (T_a - T_{opt}) \times (T_a - T_{opt})} \quad (12)$$

$$W_s = \frac{VPD_o}{VPD_o + VPD} \quad (13)$$

175 where T_{min} , T_{opt} , and T_{max} are the minimum, optimum, and maximum temperatures for vegetation photosynthesis, respectively (Yuan et al., 2007); VPD_o is the half-saturation coefficient of the VPD constraint equation (k Pa).

$APAR_{su}$ and $APAR_{sh}$ can be expressed as follows (Chen et al., 1999):

$$APAR_{su} = \left(PAR_{dir} \times \frac{\cos(\beta)}{\cos(\bar{\theta})} + \frac{PAR_{dif} - PAR_{dif,u}}{LAI} + C \right) \times LAI_{su} \quad (14)$$

$$APAR_{sh} = \left(\frac{PAR_{dif} - PAR_{dif,u}}{LAI} + C \right) \times LAI_{sh} \quad (15)$$

$$180 \quad PAR_{dif,u} = PAR_{dif} \times \exp\left(\frac{-0.5 \times \Omega \times LAI}{\cos(\bar{\theta})}\right) \quad (16)$$

where PAR_{dir} is the direct PAR; PAR_{dif} is the diffuse PAR; $PAR_{dif,u}$ is the diffuse PAR under the canopy; C represents the multiple scattering effects of direct radiation; Ω is the clumping index, which is set according to vegetation types (Tang et al., 2007); θ is the solar zenith angle; β is the mean leaf–sun angle, which is set to 60°; $\bar{\theta}$ is the representative zenith angle for diffuse radiation transmission and can be expressed by LAI (Chen et al., 1999):

$$185 \quad \cos(\bar{\theta}) = 0.537 + 0.025 \times LAI \quad (17)$$

The LAIs of shaded leaves (LAI_{sh}) and sunlit leaves (LAI_{su}) in Eqs. (14) and (15) are computed following Chen et al (1999):

$$LAI_{su} = 2 \times \cos(\theta) \times \left(1 - e^{-0.5 \times \Omega \times \frac{LAI}{\cos(\bar{\theta})}} \right) \quad (18)$$

$$LAI_{sh} = LAI - LAI_{su} \quad (19)$$

2.4 Model calibration and validation

190 Cross-validation method was used to calibrate and validate the revised EC-LUE model. Fifty percent of the sites were randomly selected to calibrate model parameters for each vegetation type, and the remaining 50% of the sites were used to validate the model. This parameterization process was repeated until all possible combinations of 50% sites were achieved for each vegetation type. The nonlinear regression procedure (Proc NLIN) in the Statistical Analysis System (SAS, SAS Institute Inc., Cary, NC, USA) was applied to optimize the model parameters (ϵ_{msu} , ϵ_{msh} , ϕ , and VPD_0) using 8-day estimated GPP based on
195 EC measurements. The mean GPP simulations of 8-day from all validation runs only were used to model validation. At global scale, mean calibrated parameter values (Table 3) were used to produce GPP dataset at $0.05^\circ \times 0.05^\circ$ spatial resolution and 8-day temporal resolution over 1982-2017. In order to investigate the uncertainties of the global GPP dataset, 10,000 sets of optimized parameters were randomly selected to simulate global GPP by assuming a normal distribution of these parameters (Table 3). The uncertainty of global GPP simulations was determined by the mean absolute deviation (MAD) of all the 10,000
200 simulations (Khair et al., 2017).

<<Table 3>>

Three metrics, the coefficient of determination (R^2), RMSE, and bias (the difference between observations and simulations) were adopted to evaluate the performance of the revised EC-LUE model. Additionally, Kendall's coefficient of rank correlation τ (Kanji, 1999) was used to quantify the agreement of seasonal changes between the simulated and tower estimated GPP. The
205 Kendall coefficient measured the tendency coherence between predicted and observed GPP by comparing the ranks assigned to successive pairs. If $GPP_{sim,j} - GPP_{sim,i}$ and $GPP_{obs,j} - GPP_{obs,i}$ have the same sign (positive or negative), the pair would be concordant, or discordant. A time-series data with n observations, the Kendall's coefficient of rank correlation τ can be expressed:

$$\tau = \frac{C-D}{n(n-1)/2} \quad (20)$$

210 where $n(n-1)/2$ is the total combination of pairs, C is the number of concordant pairs, and D is the number of discordant pairs. The Kendall's coefficient ranged from -1 (C = 0) to 1 (D = 0). The Kendall's coefficient is much closer to 1, which means a stronger positive relationship between the seasonal patterns of the simulated and tower estimated GPP.

In addition, we compared the model performance of the revised EC-LUE model with seven light use efficiency models, three machine learning methods and ten process-based ecosystem models. The participated light use efficiency models include
215 CASA (Potter et al., 1993), CFlux (Turner et al., 2006; King et al., 2011), CFix (Veroustraete et al., 2002), MODIS (Running et al., 2004), VPM (Xiao et al., 2005), VPRM (Mahadevan et al., 2008), and EC-LUE (Yuan et al., 2007). We calibrated the model parameters of all seven light use efficiency models based on the eddy covariance measurements using the same parameterization method as the revised EC-LUE model (see the above method), and then compared the GPP simulations of seven LUE models driven by EC tower-based meteorology data against the estimated GPP based on EC measurements. For
220 the comparison with machine learning models and process-based ecosystem models, we collected their global monthly GPP products released by FLUXCOM (Jung et al., 2017) and TRENDY program (version 5) (Le Quéré et al., 2016), respectively.

FLUXCOM program uses the Artificial Neural Network method (FLUXCOM ANN), the Multivariate Adaptive Regression Splines method (FLUXCOM MARS), and the Random Forest method (FLUXCOM RF); and TRENDY program includes the CSIRO Atmosphere and Biosphere Land Exchange (CABLE) (Zhang et al., 2013), the coupled Canadian Land Surface Scheme and Canadian Terrestrial Ecosystem Model (CLASS-CTEM) (Melton and Arora, 2016), the Community Land Model (CLM) (Oleson et al., 2013), the Integrated Science Assessment Model (ISAM) (Jain et al., 2013), the land component of the Max Planck Institute Earth System Model (JSBACH) (Reick et al., 2013), the Joint UK Land Environment Simulator (JULES) (Clark et al., 2011), the Lund-Postdam-Jena General Ecosystem Simulator (LPJ-GUESS) (Smith et al., 2014), the Land surface Processes and eXchanges (LPX-Bern) (Stocker et al., 2014), the ORganizing Carbon and Hydrology In Dynamic Ecosystems (ORCHIDEE) (Krinner et al., 2005), and the Vegetation Integrated Simulator for Trace Gases (VISIT) (Kato et al., 2013). The monthly GPP simulations at all investigated EC sites were derived from their global products, and equally we obtained the monthly GPP simulations of the revised EC-LUE model from its global dataset driven by MERRA-2 reanalysis dataset.

2.5 Environmental contributions to long-term changes in GPP

To evaluate the contribution of the major environmental variables to GPP, including the atmospheric CO₂ concentration ([CO₂]), climate, and satellite-based LAI, two types of experimental simulations were performed. The first simulation experiment (S_{ALL}) was a normal model run, with all the environmental drivers changing over time. In the second type of simulation experiments (S_{CLI0}, S_{LAI0}, and S_{CO20}), two driving factors could be varied with time while maintaining the third constant at an initial baseline level. For example, the S_{CLI0} simulation experiment allowed the LAI and atmospheric [CO₂] to vary with time while the climate variables were kept constant at 1982 values. The S_{LAI0} (S_{CO20}) simulation experiments kept LAI (atmospheric [CO₂]) constant at 1982 values and varied the other two variables.

Considering the differences between the simulation results of the first type (S_{ALL}) and the second type (S_{CO20} and S_{LAI0}) of experiments, the GPP sensitivities to atmospheric [CO₂] (β_{CO2}) and LAI (β_{LAI}) were estimated as follows:

$$\Delta GPP_{(S_{ALL}-S_{CO20})i} = \beta_{CO2} \times \Delta CO2_{(S_{ALL}-S_{CO20})i} + \varepsilon \quad (21)$$

$$\Delta GPP_{(S_{ALL}-S_{LAI0})i} = \beta_{LAI} \times \Delta LAI_{(S_{ALL}-S_{LAI0})i} + \varepsilon \quad (22)$$

where ΔGPP_i , $\Delta CO2_i$, and ΔLAI_i denote the differences in the GPP simulations, atmospheric [CO₂], and LAI between the two model experiments from 1982 to 2017, and ε is the stochastic error term.

The GPP sensitivities to the three climate variables: air temperature (β_{Ta}), VPD (β_{VPD}), and PAR (β_{PAR}) were calculated using a multiple regression approach:

$$\Delta GPP_{(S_{ALL}-S_{CLI0})i} = \beta_{Ta} \times \Delta Ta_{(S_{ALL}-S_{CLI0})i} + \beta_{VPD} \times \Delta VPD_{(S_{ALL}-S_{CLI0})i} + \beta_{PAR} \times \Delta PAR_{(S_{ALL}-S_{CLI0})i} + \varepsilon \quad (23)$$

where ΔTa_i , ΔVPD_i , and ΔPAR_i denote the differences in Ta, VPD, and PAR time series between the two model experiments (S_{ALL} and S_{CLI0}), respectively. The regression coefficient β was estimated using the maximum likelihood analysis.

3 Results

3.1 Model performance

255 In general, the revised EC-LUE model could effectively reproduce the spatial, seasonal, and annual variations in the tower estimated GPP at most sites (Figs. 1–3). The revised EC-LUE model explained 71% and 64% of the spatial variations in GPP across all the validation sites by using the tower-derived meteorology data and the meteorological reanalysis dataset, respectively (Fig. 1).

<<Figure 1>>

260 The revised EC-LUE model also showed a good performance in reproducing the seasonal variations in GPP at most EC sites (Fig. 2). In this study, we compared the modeled and tower GPP at 8-day step for each site to examine the model capacity in reproducing the temporal variations of GPP. In terms of GPP simulations driven by tower-derived meteorology data, the coefficients of determination (R^2) varied from 0.26 at MY-PSO site to 0.96 at DK-Sor site, with most of them being statistically significant (p -value <0.05) (Fig. 2a), and the mean R^2 was 0.81 over all investigated sites. The low R^2 values (<0.4) were found
265 at three tropical forest sites (i.e., MY-PSO, BR-Sa1 and BR-Sa3). The averaged Kendall's correlation coefficient (τ) was 0.63 over all sites, indicating a strong seasonal coherence between simulated and tower-estimated GPP (Fig. 2d). Similarly, τ at tropical forest sites were generally lower than other sites. According to the RMSE and absolute bias, the revised EC-LUE model performed very well at most sites. The averaged RMSE and absolute bias over all the sites were 2.13 and 0.81 g C m⁻² d⁻¹, respectively (Fig. 2b–c). In addition, there was no obvious difference between the seasonal GPP performances using the
270 tower-derived meteorology data and the meteorological reanalysis dataset (Fig. 2). On average, the revised EC-LUE model showed higher R^2 and τ , and lower bias and RMSE than the original EC-LUE model (Fig. 2). Furthermore, we selected three sites with high R^2 (US-UMB; DBF; $R^2 = 0.93$), median R^2 (CN-Din; EBF; $R^2 = 0.71$), and low R^2 (Br-Sa3; EBF; $R^2 = 0.39$) to illustrate the time-series changes of observed/simulated GPP, LAI, and environmental factors (i.e., air temperature, VPD, and PAR) (Figs S1-S3). At US-UMB site, the model captured the GPP variations well all the year round with no obvious bias
275 (Fig. S1). At CN-Din site, the model generally performed well except the underestimation at the end of the year (November–December) with decreased LAI (Fig. S2). While, at Br-Sa3 site, the model could not capture the variations of GPP for the vegetation greenness and environmental factors varying slightly during the year (Fig. S3).

<< Figure 2>>

The ability of the LUE models to reproduce the interannual variations in GPP was investigated at 55 EC towers with
280 observations greater than 5-years (Table 1; Fig. 3). We examined the relations between the mean annual GPP simulations and observations at each site and used the coefficient correlation (R^2) and slope of the regression relationship to investigate the model capability in simulating the interannual variations in GPP. The result showed that the revised EC-LUE model could effectively determine the interannual variations in GPP (Fig. 3). Approximately 42% and 40% of the sites showed higher R^2 values (>0.5) by using the tower-derived meteorology data and the meteorological reanalysis dataset (Fig. 3a). The averaged
285 R^2 for the revised EC-LUE model was 0.44 by using the tower-derived meteorology data, which was significantly higher than

the original EC-LUE model ($R^2 = 0.36$) and other LUE models (R^2 ranged from 0.06 to 0.30 with an average value of 0.16) (Fig. 3c). The averaged R^2 for the revised EC-LUE model was 0.42 by using the meteorological reanalysis dataset. The averaged slopes of the revised EC-LUE model were 0.60 and 0.57 by using the tower-derived meteorology data and the meteorological reanalysis dataset (Fig. 3c).

290 <<Figure 3>>

Additionally, we examined the model performance of the revised EC-LUE model, other LUE models, machine learning models, and process-based models in TRENDY at monthly step by comparing against EC tower estimated GPP (Fig. 4). In comparison with seven LUE models driven by EC tower-based meteorology dataset, the overall R^2 of the revised EC-LUE model was 0.71, higher than the original EC-LUE model and other LUE models (R^2 ranged from 0.55 to 0.61) (Fig. 4a). For each site, we compared the R^2 /RMSE/absolute value of bias of the individual model with the averaged value of all the eight LUE models (each site has an averaged R^2 /RMSE/absolute value of bias) (Fig. S4a1-c1). The revised EC-LUE model had higher R^2 than the mean R^2 of the eight LUE models at 62% sites, which was comparable with the original EC-LUE model (63% sites) and VPM model (60% sites) (Fig. S4a1). Moreover, the revised EC-LUE model showed the lower RMSE and bias compared to mean values of all eight LUE models at 68% and 67% sites respectively, which indicated the better performance compared to the other LUE models at most sites (Fig. S4b1-c1). By using the global reanalysis meteorology data, we compared the performance of the revised EC-LUE model with three existing machine learning model products and ten process-based model products in TRENDY (Fig. 4b). The overall R^2 of the revised EC-LUE model ($R^2 = 0.57$) was higher than that of other models (R^2 ranged from 0.02 to 0.54) (Fig. 4b). The revised EC-LUE model, FLUXCOM ANN, and FLUXCOM MARS had more sites (over 90%) with higher R^2 than the mean R^2 (Fig. S4a2). And the revised EC-LUE model, FLUXCOM MARS, and FLUXCOM RF showed the lower RMSE at more than 90% sites (Fig. S4b2). Compared to the other models, the revised EC-LUE model had highest site percentage (81%) with lower absolute value of bias (Fig. S4c2).

300 <<Figure 4>>

3.2 Spatial-temporal patterns of global GPP

A global GPP dataset at 0.05° latitude by 0.05° longitude and 8-day interval was generated from 1982 to 2017 based on the revised EC-LUE model. The global GPP was 106.2 ± 2.9 Pg C yr⁻¹ across the vegetated area averaged from 1982 to 2017. The GPP was high over the tropical forest areas, such as Amazon and Southeast Asia, where the moisture and temperature conditions are sufficient for photosynthesis (Fig. 5a). The GPP decreased with the decreasing gradients of temperature and precipitation (Fig. 5b). The moderate GPP was found in temperate and subhumid regions; and the lowest GPP was located in arid or cold regions, where either precipitation or temperature is limited (Fig. 5b).

315 <<Figure 5>>

Long-term trend of GPP over the period of 1982–2017 was determined using a linear regression analysis (Fig. 6). In general, the revised EC-LUE model showed an increased trend in the annual mean GPP from 1982 to 2017. Approximately 69.5% of the vegetated areas, mainly located in temperate and humid regions, showed increased trends. The spatial pattern of the GPP

trend along with the temperature and precipitation gradients was substantially heterogeneous (Fig. 6b). The decreased GPP was found in the tropic regions, especially in the Amazon forest (Fig. 6a). The extremely cold or arid areas exhibited less variations in GPP (Fig. 6b).

<<Figure 6>>

In addition, this study used the MAD of 10,000 simulations to quantify the uncertainty of estimated GPP globally (see methods). Over the globe, the mean uncertainty of estimated GPP by the revised EC-LUE model is $19.33 \text{ Pg C yr}^{-1}$. The GPP uncertainties were found to be low in high and middle latitudes, but relatively high in tropical forests (about $600 \text{ g C m}^{-2} \text{ yr}^{-1}$) (Fig. 7).

<<Figure 7>>

3.3 Contributions of environmental variables to GPP

To quantify the contributions of the environmental variables to long-term changes in GPP, we explored the sensitivity of global summed GPP to climate variables (i.e., VPD, T_a , and PAR), LAI, and atmospheric CO_2 (Fig. 8). The global summed GPP generated from different experimental simulations (section 2.5) exhibited differently in terms of the annual mean value, trend, and standard deviation (Fig. 8a). The normal simulated GPP (S_{ALL} GPP, all the environmental drivers changing over time) significantly increased at the rate of $0.15 \text{ Pg C yr}^{-1}$, while the increasing rate of S_{CLI0} GPP (climate variables were kept constant at 1982 values) was even greater ($0.41 \text{ Pg C yr}^{-1}$). On the contrary, the S_{LAI0} GPP (LAI was kept constant at 1982 values) and the S_{CO20} GPP (atmospheric $[\text{CO}_2]$ was kept constant at 1982 values) showed insignificantly decreasing trend at the rate of $-0.04 \text{ Pg C yr}^{-1}$ and $-0.07 \text{ Pg C yr}^{-1}$ (Fig. 8a). The GPP sensitivity analysis showed that the global GPP decreased by $6.67 \pm 5.04 \text{ Pg C}$ with a 0.1 kPa increase in VPD, which was comparable to the increase in GPP with 0.1 unit greening of LAI (i.e., $\beta_{\text{LAI}} = 4.78 \pm 0.72 \text{ Pg C } 0.1 \text{ unit}^{-1}$) or 100 MJ increase in PAR (i.e., $\beta_{\text{PAR}} = 5.73 \pm 3.22 \text{ Pg C } 100 \text{ MJ}^{-1}$) (Fig. 8b). The global GPP increased by $12.31 \pm 0.61 \text{ Pg C}$ with a 100 ppm^{-1} rise of atmospheric $[\text{CO}_2]$ (i.e., $\beta_{\text{CO2}} = 12.31 \pm 0.61 \text{ Pg C } 100 \text{ ppm}^{-1}$). Over the period of 1982–2017, the increased VPD resulted in the global GPP decreases of $-0.17 \pm 0.06 \text{ Pg C yr}^{-1}$, which could partly counteract the fertilization effect of CO_2 ($0.22 \pm 0.07 \text{ Pg C yr}^{-1}$). The global GPP showed a decreased trend after 2001 due to the joint effect of increased VPD and decreased PAR (Fig. 8c). While the increased trend of GPP before 2000 was affected by the rising atmospheric $[\text{CO}_2]$, greening of LAI, and increased PAR (Fig. 8c).

<<Figure 8>>

4 Discussion

4.1 Model accuracy analysis

Numerous studies have shown that most GPP models can reproduce the spatial changes in GPP but failed to reproduce the temporal variations (Keenan et al., 2012; Yuan et al., 2014). Therefore, the capacity to reproduce realistic interannual variations for a GPP model is significantly important. In our study, the revised EC-LUE model performed a higher accuracy in reproducing the interannual variations in GPP than did the original EC-LUE model and other LUE models. Yuan et al. (2014)

350 reported that the averaged slope of the regression relation between the mean annual GPP simulated by seven LUE models and the mean annual GPP estimated from EC tower ranged from 0.19 to 0.56 (Fig. 3c). While the revised EC-LUE model showed a higher slope of regression relation (0.60), which is much closer to 1 than that obtained from other LUE models (Fig. 3c). The VPM GPP showed less interannual variations across most biomes ($R^2 < 0.5$), probably because of the insensitivity of the environmental stress factors at the interannual scale (Zhang et al., 2017). In contrast, 42% of the sites showed higher R^2 values
355 (> 0.5) for the revised EC-LUE model. The improvements of the revised EC-LUE model in reproducing interannual variations are owing to the integration of several important environmental drivers for vegetation production (i.e., atmospheric CO_2 concentration, radiation components, and VPD), which exhibited large variations and contributed significantly to vegetation production at interannual scale.

By integrating the atmospheric CO_2 concentration, the revised EC-LUE model suggested a CO_2 sensitivity (β_{CO_2}) of $12.31 \pm$
360 $0.61 \text{ Pg C per } 100 \text{ ppm}$ (Fig. 8b), which indicates an increase of 11.6% in GPP with a rise of 100 ppm in atmospheric $[\text{CO}_2]$. Our estimate is comparable to the observed response of NPP to the increased CO_2 in the FACE experiments (13% per 100 ppm) and estimates of other ecosystem models (5–20% per 100 ppm) (Piao et al., 2013). The elevated atmospheric CO_2 concentration substantially contributes to vegetation productivity.

The evaporation fraction (EF), namely the ratio of evapotranspiration (ET) to net radiation (R_n), was used to indicate the water
365 stress on vegetation growth in the original EC-LUE model (Yuan et al., 2007; 2010). While the atmospheric VPD was used to indicate water stress to avoid the aggregated errors from ET simulations in the revised EC-LUE model. Physiologically, vegetation production is sensitive to both atmospheric VPD and soil moisture availability to roots. Several studies have reported highly consistent interannual variability of VPD and soil moisture (Zhou et al., 2019a, b). In addition, recent studies highlighted that the increase in VPD had a larger limitation to the surface conductance and evapotranspiration than soil
370 moisture over short time scales in many biomes (Novick et al., 2016; Sulman et al., 2016). Other studies have also suggested substantial impacts of VPD on vegetation growth (de Cárcer et al., 2018; Ding et al., 2018), forest mortality (Williams et al., 2013), and crop yields (Lobell et al., 2014). It is increasingly important to integrate the atmospheric water constraint to the carbon and water flux modeling.

4.2 Comparison of global GPP products

375 Global and regional GPP estimates remain highly uncertain despite the substantial advances in remote sensing technology, ground observations, and theory of carbon flux modeling (Zheng et al., 2018; Ryu et al., 2019). At regional scale, we compared the annual mean GPP between the revised EC-LUE model and other models across the bioclimatic zones in the Köppen-Geiger climate classification map (Beck et al., 2018) (Fig. 9). The GPP of the revised EC-LUE model was comparable to the mean value of other models for each bioclimatic zone (Fig. 9a). The GPP of different models exhibited large discrepancies in tropical
380 regions (Af/Am/Aw) (Fig. 9a). The correlations (R^2) of GPP across all the bioclimatic zones between the revised EC-LUE model and other models ranged from 0.73 (LPX-Bern) to 0.95 (FLUXCOM MARS, FLUXCOM RF) (Fig. 9b).

<<Figure 9>>

At global scale, our study showed large differences in the magnitude of global GPP estimated by various models varying from 92.7 to 168.7 Pg C yr⁻¹ (Figs. 10–11). The LUE models simulated the global GPP ranging from 92.7 to 133.7 Pg C yr⁻¹ (Fig. 11a1). Several machine learning approaches estimated the global GPP ranging from 111.0 to 144.2 Pg C yr⁻¹ (Fig. 11a2). A comparison of ten global terrestrial ecosystem models of TRENDY showed that the global GPP ranged from 107.8 to 154.9 Pg C yr⁻¹ (Fig. 11a3). The revised EC-LUE model quantified the mean global GPP from 1982 to 2017 as 106.2 ± 2.9 Pg C yr⁻¹. Other studies also support the conclusion that there are large uncertainties in the GPP estimates. By comparing diverse GPP models and products, Anav et al. (2015) reported that the global GPP ranged from 112 to 169 Pg C yr⁻¹. Seven satellite-based LUE models estimated the global GPP ranged from 95.1 to 139.7 Pg C yr⁻¹ over the period of 2000–2010 (Cai et al., 2014).

<<Figure 10>>

The interannual variability and trend in GPP also vary substantially with different models. This study showed that the interannual variability (standard deviation) ranged from 0.32 to 5.89 Pg C yr⁻¹, with the trends varying from -0.05 to 0.84 Pg C yr⁻¹ (Fig. 11). The biophysical models showed large interannual variability, with the standard deviation ranging from 1.38 to 5.89 Pg C yr⁻¹. The LUE models estimated the interannual variability varied from 1.30 to 3.13 Pg C yr⁻¹. In contrast, the machine learning models exhibited less interannual variability with standard deviation under 1.0 Pg C yr⁻¹. The interannual variability of the revised EC-LUE model was 2.9 Pg C yr⁻¹ (Figs. 11b1–b3). In general, the GPP interannual variability before the year 2000 year was greater than that after the year 2001 for most of the biophysical models and LUE models (Figs. 11b1–b3). Most GPP models showed an increased trend or insignificant trend during all valid years and before 2000. Similar to the standard deviation, the trends of machine learning models were less than other models. Compared with the other models, CLASS-CTEM and the revised EC-LUE model showed a significant decreasing trend after 2001 (Figs. 11c1–c3), probably because of the joint effect of increased VPD and decreased PAR (Fig. 8c).

<<Figure 11>>

4.3 Model uncertainty

The uncertainties of our GPP dataset were low in high and middle latitude areas but high in tropical areas (Fig. 7). This is consistent with the validations at site level that the revised EC-LUE model showed the lowest accuracy over the tropical evergreen broadleaf forest sites (Fig. 2). Similarly, other satellite-based models exhibited a large uncertainty in the GPP simulations over tropical forest areas (Ryu et al., 2011; Yuan et al., 2014). For example, MODIS GPP product (MOD17) underestimated GPP at high productivity sites over the tropical evergreen forests (de Almeida et al., 2018). Regarding the quality of satellite data, a high cloud cover exists over tropical regions, introducing large uncertainties to FAPAR/LAI and other vegetation indices (e.g., NDVI and EVI). As suggested by de Almeida et al. (2018), the lack of reliable MOD15 FAPAR data during January to April as a result of the cloudiness contamination could have substantially affected the seasonality of GPP estimates. Besides, the quality of satellite data can even affect the evaluation of the interannual variations in GPP. Using MODIS EVI data, Saleska et al. (2007) reported a large-scale green up in the Amazon evergreen forests during the drought of

2005. However, an opposite conclusion was drawn when the cloud-contaminated data were excluded from the analysis (Samanta et al., 2010). In our study, a significant decrease of GPP was found in the Amazon evergreen forests, which may be resulted from the sharp increase in VPD after the late 1990s (Yuan et al., 2019). Studies using optical satellite data can be influenced by the cloudiness contamination. Recently studies using cloud free satellite-based microwave data also reported a
420 carbon loss in tropic forest (Liu et al., 2015; Fan et al., 2019).

The latest study highlighted that the aggregate canopy phenology rather than the climate changes is the main cause of the seasonal changes in photosynthesis in evergreen broadleaf forests (Wu et al., 2016). In particular, the new leaf growing synchronously with dry season litterfall may shift the old canopy to be younger, which can explain the significant seasonal increase (~27%) in the ecosystem photosynthesis. Therefore, the vertical changes in leaf age and photosynthesis ability with
425 canopy depth are important to simulate the seasonal variations in carbon flux in tropical forests (Wu et al., 2017). These leaf trait related parameters can be simulated from the narrow-band spectra of leaves (Serbin et al., 2012; Dechant et al., 2017). Nevertheless, because of the limitation in obtaining the large scale hyperspectral remote sensing data, regional or global estimation of these parameters are currently unavailable.

The revised EC-LUE model does not integrate the regulation of soil nitrogen content on vegetation production. Atmospheric
430 nitrogen deposition has exhibited a large increasing trend in the past few decades because of the excessive fossil fuel combustion in the industrial and transportation sectors and the abuse of nitrogenous fertilizer in the agricultural practice (Galloway et al., 2004). And the global land atmospheric nitrogen deposition is expected to further increase dramatically from 25–40 Tg N yr⁻¹ in the 2000s to 60–100 Tg N yr⁻¹ in 2100 (Lamarque et al., 2005). A meta-analysis of worldwide nitrogen addition experiments found that nitrogen addition could have a significantly positive effect on vegetation productivity (Liu
435 and Greaver, 2009). As most terrestrial ecosystems are nitrogen limited, quantifying the spatio-temporal distributions of vegetation nitrogen content at large scales is essential to improve the accuracy of carbon flux estimation. Several studies quantified the leaf nitrogen content by detecting the nitrogen absorption spectra from the narrow-band of hyperspectral data (Cho, 2007). However, leaf water, starch, lignin, and cellulose overlap with the absorption characters of nitrogen in the shortwave infrared bands, making it difficult to retrieve the nitrogen content (Kokaly and Clark, 1999). Additionally, canopy
440 structures, background, and illumination/viewing geometry can further decrease the capacity to detect leaf nitrogen (Yoder and Pettigrew-Crosby, 1995; Knyazikhin et al., 2013). Advances in inversion and statistical models of leaf or canopy nitrogen have emerged (Asner et al., 2011; Dechant et al., 2017; Wang et al., 2018), but these methods require further evaluation over large regions and the global map of leaf or canopy nitrogen is not available yet.

Additionally, the uncertainty of the revised EC-LUE model may arise by scale mismatches between eddy covariance flux
445 footprint and input dataset. The eddy covariance flux footprint is generally less than 3 km² and varies depending on the wind speed, wind direction and atmospheric stability (Tan et al., 2006). In our studies, the revised EC-LUE model was run at 0.05 degree (~5 km²) spatial resolution. The uncertainty of simulated GPP introduced by the scale effect is inevitable but smaller than that introduced by the model structures, parameters or input datasets (Sjostrom et al., 2013; Zheng et al., 2018).

5 Data availability

450 The $0.05^\circ \times 0.05^\circ$ global GPP dataset for 1982-2017 is available at <https://doi.org/10.6084/m9.figshare.8942336> (Zheng et al., 2019). The dataset is provided in hdf format at 8-day interval. The valid value is ranged from 0 to 3000, and the background filled value is 65535. The scale factor of the data is 0.01. Each hdf file represents an 8-day GPP at daily value (unit: $\text{g C m}^{-2} \text{ day}^{-1}$). To obtain the summation of each 8-day (or 5-day or 6-day) period, please multiply the GPP value by corresponding days (8 for the first 45 values, and 5 or 6 for the last value in a year).

455 6 Conclusion

In this study, we produced a long-term global GPP dataset by integrating several major long-term environmental variables into a light use efficiency model, including atmospheric CO_2 concentration, radiation components, and atmospheric water vapor pressure. These environmental variables showed substantial long-term changes and contributed significantly to vegetation production at interannual scale. The revised EC-LUE performed well in simulating the spatial, seasonal, and interannual
460 variations in GPP across the globe. Particularly, it has a unique superiority in reproducing the interannual variations in GPP ($R^2 = 0.44$) compared with the original EC-LUE model ($R^2 = 0.36$) and other LUE models (R^2 ranged from 0.06 to 0.30 with an average value of 0.16). The GPP dataset derived from the revised EC-LUE model provides an alternative and reliable estimates of global GPP at the long-term scale by integrating the important environmental variables.

Author contributions. W. Yuan and Y. Zheng designed the research, performed the analysis, and wrote the paper; R. Shen,
465 Y. Wang, and X. Li performed the analysis; S. Liu, S. Liang, J. Chen, W. Ju, and L. Zhang edited and revised the manuscript.

Competing interests. The authors declare that they have no conflict of interest.

Acknowledgements

This study was supported by National Key Basic Research Program of China (2016YFA0602701), Changjiang Young Scholars Programme of China (Q2016161), Training Project of Sun Yat-sen University (16lgjc53), Fok Ying Tung Education
470 Foundation (151015), and Beijing Normal University Project (2015KJJCA14). The covariance data used in the study was acquired and shared by the FLUXNET community, including these networks: AmeriFlux, AfriFlux, AsiaFlux, CarboAfrica, CarboEuropeIP, CarboItaly, CarboMont, ChinaFlux, Fluxnet-Canada, GreenGrass, ICOS, KoFlux, LBA, NECC, OzFlux-TERN, TCOS-Siberia, and USCCC. The ERA-Interim reanalysis data are provided by ECMWF and processed by LSCE. The FLUXNET eddy covariance data processing and harmonization was carried out by the European Fluxes Database Cluster,
475 AmeriFlux Management Project, and Fluxdata project of FLUXNET, with the support of CDIAC and ICOS Ecosystem Thematic Center, and the OzFlux, ChinaFlux and AsiaFlux offices.

References

- Ainsworth, E.A., Long, S.P.: What have we learned from 15 years of free-air CO₂ enrichment (FACE)? A meta-analytic review of the responses of photosynthesis, canopy, *New Phytol.*, 165, 351-371, doi:10.1111/j.1469-8137.2004.01224.x, 2005.
- 480 Alton, P.B., North, P.R., Los, S.O.: The impact of diffuse sunlight on canopy light-use efficiency, gross photosynthetic product and net ecosystem exchange in three forest biomes, *Global Change Biol.*, 13, 776-787, doi:10.1111/j.1365-2486.2007.01316.x, 2007.
- Anav, A., Friedlingstein, P., Beer, C., Ciais, P., Harper, A., Jones, C., Murray-Tortarolo, G., Papale, D., Parazoo, N.C., Peylin, P., Piao, S., Sitch, S., Viovy, N., Wiltshire, A., Zhao, M.: Spatiotemporal patterns of terrestrial gross primary production: A
485 review, *Rev. Geophys.*, 53, 785-818, doi:10.1002/2015rg000483, 2015.
- Asner, G.P., Martin, R.E., Knapp, D.E., Tupayachi, R., Anderson, C., Carranza, L., Martinez, P., Houcheime, M., Sinca, F., Weiss, P.: Spectroscopy of canopy chemicals in humid tropical forests, *Remote Sens. Environ.*, 115, 3587-3598, doi:10.1016/j.rse.2011.08.020, 2011.
- Beck, H.E., Zimmermann, N.E., McVicar, T.R., Vergopolan, N., Berg, A., Wood, E.F.: Present and future Koppen-Geiger
490 climate classification maps at 1-km resolution, *Scientific Data*, doi:510.1038/sdata.2018.214, 2018.
- Cai, W., Yuan, W., Liang, S., Zhang, X., Dong, W., Xia, J., Fu, Y., Chen, Y., Liu, D., Zhang, Q.: Improved estimations of gross primary production using satellite-derived photosynthetically active radiation, *J. Geophys. Res. G: Biogeosci.*, 119, 110-123, doi:10.1002/2013jg002456, 2014.
- Cai, W., Yuan, W., Liang, S., Liu, S., Dong, W., Chen, Y., Liu, D., Zhang, H.: Large Differences in Terrestrial Vegetation
495 Production Derived from Satellite-Based Light Use Efficiency Models, *Remote Sens.*, 6, 8945-8965, doi:10.3390/rs6098945, 2014.
- Canadell, J.G., Le Quere, C., Raupach, M.R., Field, C.B., Buitenhuis, E.T., Ciais, P., Conway, T.J., Gillett, N.P., Houghton, R.A., Marland, G.: Contributions to accelerating atmospheric CO₂ growth from economic activity, carbon intensity, and efficiency of natural sinks, *Proc. Natl. Acad. Sci. U.S.A.*, 104, 18866-18870, doi:10.1073/pnas.0702737104, 2007.
- 500 Chen, J.M., Liu, J., Cihlar, J., Goulden, M.L.: Daily canopy photosynthesis model through temporal and spatial scaling for remote sensing applications, *Ecol. Modell.*, 124, 99-119, doi:10.1016/s0304-3800(99)00156-8, 1999.
- Cho, M.A., Skidmore, A., Corsi, F., van Wieren, S.E., Sobhan, I.: Estimation of green grass/herb biomass from airborne hyperspectral imagery using spectral indices and partial least squares regression, *International Journal of Applied Earth Observation and Geoinformation*, 9, 414-424, doi:10.1016/j.jag.2007.02.001, 2007.
- 505 Clark, D. B., Mercado, L. M., Sitch, S., Jones, C. D., Gedney, N., Best, M. J., Pryor, M., Rooney, G. G., Essery, R. L. H., Blyth, E., Boucher, O., Harding, R. J., Huntingford, C., and Cox, P. M.: The Joint UK Land Environment Simulator (JULES), model description – Part 2: Carbon fluxes and vegetation dynamics, *Geosci. Model Dev.*, 4, 701–722, doi:10.5194/gmd-4-701-2011, 2011.

- Collatz, G.J., Ball, J.T., Grivet, C., Berry, J.A.: Physiological and environmental regulation of stomatal conductance, photosynthesis and transpiration: a model that includes a laminar boundary layer, *Agric. For. Meteorol.*, 54, 107-136, 1991.
- 510 de Almeida, C.T., Delgado, R.C., Galvao, L.S., de Oliveira Cruz e Aragao, L.E., Concepcion Ramos, M.: Improvements of the MODIS Gross Primary Productivity model based on a comprehensive uncertainty assessment over the Brazilian Amazonia, *ISPRS J. Photogramm. Remote Sens.*, 145, 268-283, doi:10.1016/j.isprsjprs.2018.07.016, 2018.
- de Cárcer, P.S., Vitasse, Y., Peñuelas, J., Jasey, V.E.J., Buttler, A., Signarbieux, C.: Vapor-pressure deficit and extreme climatic variables limit tree growth, *Global Change Biol.*, 24, 1108-1122, doi:10.1111/gcb.13973, 2018.
- 515 Dechant, B., Cuntz, M., Vohland, M., Schulz, E., Doktor, D.: Estimation of photosynthesis traits from leaf reflectance spectra: Correlation to nitrogen content as the dominant mechanism, *Remote Sens. Environ.*, 196, 279-292, doi:10.1016/j.rse.2017.05.019, 2017.
- Ding, J., Yang, T., Zhao, Y., Liu, D., Wang, X., Yao, Y., Peng, S., Wang, T., Piao, S.: Increasingly Important Role of Atmospheric Aridity on Tibetan Alpine Grasslands, *Geophys. Res. Lett.*, 45, 2852-2859, doi:10.1002/2017gl076803, 2018.
- 520 Fan, L., Wigneron, J.-P., Ciaïis, P., Chave, J., Brandt, M., Fensholt, R., Saatchi, S. S., Bastos, A., Al-Yaari, A., Hufkens, K., Qin, Y., Xiao, X., Chen, C., Myneni, R. B., Fernandez-Moran, R., Mialon, A., Rodriguez-Fernandez, N. J., Kerr, Y., Tian, F., and Penuelas, J.: Satellite-observed pantropical carbon dynamics, *Nature Plants*, 5, 944-951, 2019.
- Farquhar, G.D., von Caemmerer, S., Berry, J.A.: A biochemical model of photosynthetic CO₂ assimilation in leaves of C₃ species, *Planta*, 149, 78-90, doi:10.1007/bf00386231, 1980.
- 525 Fletcher, A.L., Sinclair, T.R., Allen, L.H.: Transpiration responses to vapor pressure deficit in well watered 'slow-wilting' and commercial soybean, *Environ. Exp. Bot.*, 61, 145-151, doi:10.1016/j.envexpbot.2007.05.004, 2007.
- Galloway, J.N., Dentener, F.J., Capone, D.G., Boyer, E.W., Howarth, R.W., Seitzinger, S.P., Asner, G.P., Cleveland, C.C., Green, P.A., Holland, E.A., Karl, D.M., Michaels, A.F., Porter, J.H., Townsend, A.R., Vorosmarty, C.J.: Nitrogen cycles: past, present, and future, *Biogeochemistry*, 70, 153-226, doi:10.1007/s10533-004-0370-0, 2004.
- 530 Gilgen, H., Wild, M., Ohmura, A.: Means and trends of shortwave irradiance at the surface estimated from Global Energy Balance Archive data, *J. Clim.*, 11, 2042-2061, doi:10.1175/1520-0442-11.8.2042, 1998.
- Gu, L.H., Baldocchi, D., Verma, S.B., Black, T.A., Vesala, T., Falge, E.M., Dowty, P.R.: Advantages of diffuse radiation for terrestrial ecosystem productivity, *J. Geophys. Res. D: Atmos.*, 10710.1029/2001jd001242, 2002.
- 535 Kanniah, K.D., Beringer, J., North, P., Hutley, L.: Control of atmospheric particles on diffuse radiation and terrestrial plant productivity: A review, *Progress in Physical Geography-Earth and Environment*, 36, 209-237, doi:10.1177/0309133311434244, 2012.
- Ju, W., Chen, J.M., Black, T.A., Barr, A.G., Liu, J., Chen, B.: Modelling multi-year coupled carbon and water fluxes in a boreal aspen forest, *Agric. For. Meteorol.*, 140, 136-151, doi:10.1016/j.agrformet.2006.08.008, 2006.
- 540 Jain, A. K., Meiyappan, P., Song, Y., and House, J. I.: CO₂ Emissions from Land-Use Change Affected More by Nitrogen Cycle, than by the Choice of Land Cover Data, *Glob. Change Biol.*, 9, 2893-2906, 2013.

- Jung, M., Reichstein, M., Schwalm, C.R., Huntingford, C., Sitch, S., Ahlstrom, A., Arneeth, A., Camps-Valls, G., Ciais, P., Friedlingstein, P., Gans, F., Ichii, K., Ain, A.K.J., Kato, E., Papale, D., Poulter, B., Raduly, B., Rodenbeck, C., Tramontana, G., Viovy, N., Wang, Y.-P., Weber, U., Zaehle, S., Zeng, N.: Compensatory water effects link yearly global land CO₂ sink changes to temperature, *Nature*, 541, 516-520, doi:10.1038/nature20780, 2017.
- 545 Kanji, G.K., 1999. 100 Statistical Tests. SAGE Publications, London.
- Kato, E., Kinoshita, T., Ito, A., Kawamiya, M., and Yamagata, Y.: Evaluation of spatially explicit emission scenario of land-use change and biomass burning using a process-based biogeochemical model, *Journal of Land Use Science*, 8, 104–122, 2013.
- Keenan, T.F., Baker, I., Barr, A., Ciais, P., Davis, K., Dietze, M., Dragon, D., Gough, C.M., Grant, R., Hollinger, D., Hufkens, K., Poulter, B., McCaughey, H., Raczka, B., Ryu, Y., Schaefer, K., Tian, H., Verbeeck, H., Zhao, M., Richardson, A.D.: Terrestrial biosphere model performance for inter-annual variability of land-atmosphere CO₂ exchange, *Global Change Biol.*, 18, 1971-1987, doi:10.1111/j.1365-2486.2012.02678.x, 2012.
- 550 Keenan, T.F., Prentice, I.C., Canadell, J.G., Williams, C.A., Wang, H., Raupach, M., Collatz, G.J.: Recent pause in the growth rate of atmospheric CO₂ due to enhanced terrestrial carbon uptake, *Nat. Commun.*, 7, 1038/ncomms13428, 2016.
- Khair U., Fahmi H., Al Hakim S., Rahim R.: Forecasting Error Calculation with Mean Absolute Deviation and Mean Absolute Percentage Error. In *Journal of Physics: Conference Series*, vol. 930, No. 1, p. 012002. IOP Publishing, 2017.
- King, D.A., Turner, D.P., Ritts, W.D.: Parameterization of a diagnostic carbon cycle model for continental scale application, *Remote Sens. Environ.*, 1157, 1653–1664, 2011.
- Knyazikhin, Y., Schull, M.A., Stenberg, P., Mottus, M., Rautiainen, M., Yang, Y., Marshak, A., Latorre Carmona, P., Kaufmann, R.K., Lewis, P., Disney, M.I., Vanderbilt, V., Davis, A.B., Baret, F., Jacquemoud, S., Lyapustin, A., Myneni, R.B.: Hyperspectral remote sensing of foliar nitrogen content, *Proc. Natl. Acad. Sci. U.S.A.*, 110, E185-E192, doi:10.1073/pnas.1210196109, 2013.
- 560 Kokaly, R.F., Clark, R.N.: Spectroscopic determination of leaf biochemistry using band-depth analysis of absorption features and stepwise multiple linear regression, *Remote Sens. Environ.*, 67, 267-287, doi:10.1016/s0034-4257(98)00084-4, 1999.
- Konings, A.G., Williams, A.P., Gentine, P.: Sensitivity of grassland productivity to aridity controlled by stomatal and xylem regulation, *Nat. Geosci.*, 10, 284+, doi:10.1038/ngeo2903, 2017.
- Korson, L., Drost-Hansen, W., Millero, F.J.: Viscosity of water at various temperatures, *J. Phys. Chem.*, 73, 34-39, doi:10.1021/j100721a006, 1969.
- Krinner, G., Viovy, N., de Noblet, N., Ogée, J., Friedlingstein, P., Ciais, P., Sitch, S., Polcher, J., and Prentice, I. C.: A dynamic global vegetation model for studies of the coupled atmosphere-biosphere system, *Global Biogeochem. Cy.*, 19, 1–33, 2005.
- 570 Krupkova, L., Markova, I., Havrankova, K., Pokorny, R., Urban, O., Sigut, L., Pavelka, M., Cienciala, E., Marek, M.V.: Comparison of different approaches of radiation use efficiency of biomass formation estimation in Mountain Norway spruce, *Trees-Structure and Function*, 31, 325-337, doi:10.1007/s00468-016-1486-2, 2017.
- Lamarque, J.F., Kiehl, J.T., Brasseur, G.P., Butler, T., Cameron-Smith, P., Collins, W.D., Collins, W.J., Granier, C., Hauglustaine, D., Hess, P.G., Holland, E.A., Horowitz, L., Lawrence, M.G., McKenna, D., Merilees, P., Prather, M.J., Rasch,
- 575

- P.J., Rotman, D., Shindell, D., Thornton, P.: Assessing future nitrogen deposition and carbon cycle feedback using a multimodel approach: Analysis of nitrogen deposition, *J. Geophys. Res. D: Atmos.*, 11010.1029/2005jd005825, 2005.
- Le Quéré, C., Andrew, R. M., Canadell, J. G., Sitch, S., Korsbakken, J. I., Peters, G. P., Manning, A. C., Boden, T. A., Tans, P. P., Houghton, R. A., Keeling, R. F., Alin, S., Andrews, O. D., Anthoni, P., Barbero, L., Bopp, L., Chevallier, F., Chini, L.,
580 P., Ciais, P., Currie, K., Delire, C., Doney, S. C., Friedlingstein, P., Gkritzalis, T., Harris, I., Hauck, J., Haverd, V., Hoppema, M., Klein Goldewijk, K., Jain, A. K., Kato, E., Körtzinger, A., Landschützer, P., Lefèvre, N., Lenton, A., Lienert, S., Lombardozzi, D., Melton, J. R., Metz, N., Miller, F., Monteiro, P. M. S., Munro, D. R., Nabel, J. E. M. S., Nakaoka, S., O'Brien, K., Olsen, A., Omar, A. M., Ono, T., Pierrot, D., Poulter, B., Rödenbeck, C., Salisbury, J., Schuster, U., Schwinger, J., Séférian, R., Skjelvan, I., Stocker, B. D., Sutton, A. J., Takahashi, T., Tian, H., Tilbrook, B., van der Laan-Luijkx, I. T., van
585 der Werf, G. R., Viovy, N., Walker, A. P., Wiltshire, A. J., and Zaehle, S.: Global Carbon Budget 2016, *Earth Syst. Sci. Data*, 8, 605–649, <https://doi.org/10.5194/essd-8-605-2016>, 2016.
- Li, X.L., Liang, S.L., Yu, G.R., Yuan, W.P., Cheng, X., Xia, J.Z., Zhao, T.B., Feng, J.M., Ma, Z.G., Ma, M.G., Liu, S.M., Chen, J.Q., Shao, C.L., Li, S.G., Zhang, X.D., Zhang, Z.Q., Chen, S.P., Ohta, T., Varlagin, A., Miyata, A., Takagi, K., Saiqusa, N., Kato, T.: Estimation of gross primary production over the terrestrial ecosystems in China, *Ecol. Modell.*, 261, 80-92,
590 doi:10.1016/j.ecolmodel.2013.03.024, 2013.
- Liu, L., Greaver, T.L.: A review of nitrogen enrichment effects on three biogenic GHGs: the CO₂ sink may be largely offset by stimulated N₂O and CH₄ emission, *Ecol. Lett.*, 12, 1103-1117, doi:10.1111/j.1461-0248.2009.01351.x, 2009.
- Liu, S., Bond-Lamberty, B., Boyesen, L.R., Ford, J.D., Fox, A., Gallo, K., Hatfield, J., Henebry, G.M., Huntington, T.G., Liu, Z., Loveland, T.R., Norby, R.J., Sohl, T., Steiner, A.L., Yuan, W., Zhang, Z., Zhao, S.: Grand Challenges in Understanding
595 the Interplay of Climate and Land Changes, *Earth Interactions*, 21, 1-43, doi:10.1175/ei-d-16-0012.1, 2017.
- Liu, Y., Xiao, J., Ju, W., Zhu, G., Wu, X., Fan, W., Li, D., Zhou, Y.: Satellite-derived LAI products exhibit large discrepancies and can lead to substantial uncertainty in simulated carbon and water fluxes, *Remote Sens. Environ.*, 206, 174-188, doi:10.1016/j.rse.2017.12.024, 2018.
- Liu, Y. Y., van Dijk, A. I. J. M., de Jeu, R. A. M., Canadell, J. G., McCabe, M. F., Evans, J. P., and Wang, G.: Recent reversal
600 in loss of global terrestrial biomass, *Nat. Clim. Change*, 5, 470-474, 2015.
- Lobell, D.B., Roberts, M.J., Schlenker, W., Braun, N., Little, B.B., Rejesus, R.M., Hammer, G.L.: Greater Sensitivity to Drought Accompanies Maize Yield Increase in the US Midwest, *Science*, 344, 516-519, doi:10.1126/science.1251423, 2014.
- Monteith, J.: Solar radiation and productivity in tropical ecosystems, *J. Appl. Ecol.*, 9, 747-766, 1972.
- Mahadevan, P., Wofsy, S.C., Matross, D.M., Xiao, X.M., Dunn, A.L., Lin, J.C., Gerbig, C., Munger, J.W., Chow, V.Y.,
605 Gottlieb, E.W.: A satellite-based biosphere parameterization for net ecosystem CO₂ exchange: Vegetation Photosynthesis and Respiration Model VPRM, *Global Biogeochem. Cycles*, 222, 1–17, 2008.
- Melton, J. R. and Arora, V. K.: Competition between plant functional types in the Canadian Terrestrial Ecosystem Model (CTEM) v. 2.0, *Geosci. Model Dev.*, 9, 323–361, doi:10.5194/gmd-9-323-2016, 2016.

- Norby, R.J., DeLucia, E.H., Gielen, B., Calfapietra, C., Giardina, C.P., King, J.S., Ledford, J., McCarthy, H.R., Moore, D.J.P.,
610 Ceulemans, R., De Angelis, P., Finzi, A.C., Karnosky, D.F., Kubiske, M.E., Lukac, M., Pregitzer, K.S., Scarascia-Mugnozza,
G.E., Schlesinger, W.H., Oren, R.: Forest response to elevated CO₂ is conserved across a broad range of productivity, *Proc.
Natl. Acad. Sci. U.S.A.*, 102, 18052-18056, doi:10.1073/pnas.0509478102, 2005.
- Norby, R.J., Wullschlegel, S.D., Gunderson, C.A., Johnson, D.W., Ceulemans, R.: Tree responses to rising CO₂ in field
experiments: implications for the future forest, *Plant Cell Environ.*, 22, 683-714, doi:10.1046/j.1365-3040.1999.00391.x, 1999.
- 615 Novick, K.A., Ficklin, D.L., Stoy, P.C., Williams, C.A., Bohrer, G., Oishi, A.C., Papuga, S.A., Blanken, P.D., Noormets, A.,
Sulman, B.N., Scott, R.L., Wang, L., Phillips, R.P.: The increasing importance of atmospheric demand for ecosystem water
and carbon fluxes, *Nat. Clim. Change*, 6, 1023-1027, doi:10.1038/nclimate3114, 2016.
- Oleson, K. W., Lawrence, D. M., Bonan, G. B., Drewniak, B., Huang, M., Koven, C. D., Levis, S., Li, F., Riley, W. J., Subin,
Z. M., Swenson, S. C., Thornton, P. E., Bozbiyik, A., Fisher, R., Heald, C. L., Kluzek, E., Lamarque, J., Lawrence, P. J., Leung,
620 L. R., Lipscomb, W., Muszala, S., Ricciuto, D. M., Sacks, W., Tang, J., and Yang, Z.: Technical Description of version 4.5 of
the Community Land Model (CLM), National Center for Atmospheric Research, Boulder, CO, USA, available at:
http://www.cesm.ucar.edu/models/cesm1.2/clm/CLM45_Tech_Note.pdf, 2013.
- Piao, S., Sitch, S., Ciais, P., Friedlingstein, P., Peylin, P., Wang, X., Ahlstrom, A., Anav, A., Canadell, J.G., Cong, N.,
Huntingford, C., Jung, M., Levis, S., Levy, P.E., Li, J., Lin, X., Lomas, M.R., Lu, M., Luo, Y., Ma, Y., Myneni, R.B., Poulter,
625 B., Sun, Z., Wang, T., Viovy, N., Zaehle, S., Zeng, N.: Evaluation of terrestrial carbon cycle models for their response to
climate variability and to CO₂ trends, *Global Change Biol.*, 19, 2117-2132, doi:10.1111/gcb.12187, 2013.
- Pierce, D.W., Westerling, A.L., Oyler, J.: Future humidity trends over the western United States in the CMIP5 global climate
models and variable infiltration capacity hydrological modeling system, *Hydrol. Earth Syst. Sci.*, 17, 1833-1850,
doi:10.5194/hess-17-1833-2013, 2013.
- 630 Potter, C.S., Randerson, J.T., Field, C.B., Matson, P.A., Vitousek, P.M., Mooney, H.A., Klooster, S.A.: Terrestrial ecosystem
production: A process model-based on global satellite and surface data, *Global Biogeochem. Cycles*, 7, 811-841,
doi:10.1029/93gb02725, 1993.
- Prentice, I.C., Dong, N., Gleason, S.M., Maire, V., Wright, I.J.: Balancing the costs of carbon gain and water transport: testing
a new theoretical framework for plant functional ecology, *Ecol. Lett.*, 17, 82-91, doi:10.1111/ele.12211, 2014.
- 635 Rawson, H.M., Begg, J.E., Woodward, R.G.: The effect of atmospheric humidity on photosynthesis, transpiration and water
use efficiency of leaves of several plant species, *Planta*, 134, 5-10, doi:10.1007/bf00390086, 1977.
- Reichstein, M., Falge, E., Baldocchi, D., Papale, D., Aubinet, M., Berbigier, P., Bernhofer, C., Buchmann, N., Gilmanov, T.,
Granier, A., Grunwald, T., Havrankova, K., Ilvesniemi, H., Janous, D., Knohl, A., Laurila, T., Lohila, A., Loustau, D.,
Matteucci, G., Meyers, T., Miglietta, F., Ourcival, J.-M., Pumpanen, J., Rambal, S., Rotenberg, E., Sanz, M., Tenhunen, J.,
640 Seufert, G., Vaccari, F., Vesala, T., Yakir, D., Valentini, R.: On the separation of net ecosystem exchange into assimilation
and ecosystem respiration: review and improved algorithm, *Global Change Biol.*, 11, 1424-1439, doi:10.1111/j.1365-
2486.2005.001002.x, 2005.

- Reick, C. H., T. Raddatz, V. Brovkin, and Gayler, V.: The representation of natural and anthropogenic land cover change in MPIESM, *J. Adv. Model. Earth Syst.*, 5, 459–482, 2013.
- 645 Rienecker, M.M., Suarez, M.J., Gelaro, R., Todling, R., Bacmeister, J., Liu, E., Bosilovich, M.G., Schubert, S.D., Takacs, L., Kim, G.-K., Bloom, S., Chen, J., Collins, D., Conaty, A., Da Silva, A., Gu, W., Joiner, J., Koster, R.D., Lucchesi, R., Molod, A., Owens, T., Pawson, S., Pegion, P., Redder, C.R., Reichle, R., Robertson, F.R., Ruddick, A.G., Sienkiewicz, M., Woollen, J.: MERRA: NASA's modern-era retrospective analysis for research and applications, *J. Clim.*, 24, 3624–3648, doi:10.1175/jcli-d-11-00015.1, 2011.
- 650 Running, S.W., Nemani, R.R., Heinsch, F.A., Zhao, M.S., Reeves, M., Hashimoto, H.: A continuous satellite-derived measure of global terrestrial primary production, *Bioscience*, 54, 547–560, doi:10.1641/0006-3568(2004)054[0547:acsmog]2.0.co;2, 2004.
- Ryu, Y., Baldocchi, D.D., Kobayashi, H., van Ingen, C., Li, J., Black, T.A., Beringer, J., van Gorsel, E., Knohl, A., Law, B.E., Rouspard, O.: Integration of MODIS land and atmosphere products with a coupled-process model to estimate gross primary productivity and evapotranspiration from 1 km to global scales, *Global Biogeochem. Cycles*, 2510.1029/2011gb004053, 2011.
- 655 Ryu, Y., Berry, J.A., Baldocchi, D.D.: What is global photosynthesis? History, uncertainties and opportunities, *Remote Sens. Environ.*, 223, 95–114, doi:10.1016/j.rse.2019.01.016, 2019.
- Saleska, S.R., Didan, K., Huete, A.R., da Rocha, H.R.: Amazon forests green-up during 2005 drought, *Science*, 318, 612–612, doi:10.1126/science.1146663, 2007.
- 660 Samanta, A., Ganguly, S., Hashimoto, H., Devadiga, S., Vermote, E., Knyazikhin, Y., Nemani, R.R., Myneni, R.B.: Amazon forests did not green-up during the 2005 drought, *Geophys. Res. Lett.*, 3710.1029/2009gl042154, 2010.
- Serbin, S.P., Dillaway, D.N., Kruger, E.L., Townsend, P.A.: Leaf optical properties reflect variation in photosynthetic metabolism and its sensitivity to temperature, *J. Exp. Bot.*, 63, 489–502, doi:10.1093/jxb/err294, 2012.
- Simmons, A.J., Willett, K.M., Jones, P.D., Thorne, P.W., Dee, D.P.: Low-frequency variations in surface atmospheric humidity, temperature, and precipitation: Inferences from reanalyses and monthly gridded observational data sets, *J. Geophys. Res. D: Atmos.*, 11510.1029/2009jd012442, 2010.
- 665 Sjoström, M., Zhao, M., Archibald, S., Arneth, A., Cappelaere, B., Falk, U., de Grandcourt, A., Hanan, N., Kergoat, L., Kutsch, W., Merbold, L., Mougin, E., Nickless, A., Nouvellon, Y., Scholes, R.J., Veenendaal, E.M., Ardo, J.: Evaluation of MODIS gross primary productivity for Africa using eddy covariance data, *Remote Sens. Environ.*, 131, 275–286, doi:10.1016/j.rse.2012.12.023, 2013.
- 670 Smith, B., Wårlind, D., Arneth, A., Hickler, T., Leadley, P., Siltberg, J., and Zaehle, S.: Implications of incorporating N cycling and N limitations on primary production in an individualbased dynamic vegetation model, *Biogeosciences*, 11, 2027–2054, doi:10.5194/bg-11-2027-2014, 2014.
- Smith, W.K., Reed, S.C., Cleveland, C.C., Ballantyne, A.P., Anderegg, W.R.L., Wieder, W.R., Liu, Y.Y., Running, S.W.: Large divergence of satellite and Earth system model estimates of global terrestrial CO₂ fertilization, *Nat. Clim. Change*, 6, 306–310, doi:10.1038/nclimate2879, 2016.

- Stocker, B. D., Feissli, F., Strassmann, K. M., Spahni, R., and Joos, F.: Past and future carbon fluxes from land use change, shifting cultivation and wood harvest, *Tellus B*, 66, 23188, doi:10.3402/tellusb.v66.23188, 2014.
- 680 Stocker, B.D., Zscheischler, J., Keenan, T.F., Prentice, I.C., Seneviratne, S.I., Peñuelas, J.: Drought impacts on terrestrial primary production underestimated by satellite monitoring, *Nat. Geosci.*, 12, 264-270, doi:10.1038/s41561-019-0318-6, 2019.
- Sulman, B.N., Roman, D.T., Yi, K., Wang, L., Phillips, R.P., Novick, K.A.: High atmospheric demand for water can limit forest carbon uptake and transpiration as severely as dry soil, *Geophys. Res. Lett.*, 43, 9686-9695, doi:10.1002/2016gl069416, 2016.
- 685 Tan, B., Woodcock, C.E., Hu, J., Zhang, P., Ozdogan, M., Huang, D., Yang, W., Knyazikhin, Y., Myneni, R.B.: The impact of gridding artifacts on the local spatial properties of MODIS data: Implications for validation, compositing, and band-to-band registration across resolutions, *Remote Sens. Environ.*, 105, 98-114, doi:10.1016/j.rse.2006.06.008, 2006.
- Tang, S., Chen, J.M., Zhu, Q., Li, X., Chen, M., Sun, R., Zhou, Y., Deng, F., Xie, D.: LAI inversion algorithm based on directional reflectance kernels, *J. Environ. Manage.*, 85, 638-648, doi:10.1016/j.jenvman.2006.08.018, 2007.
- 690 Turner, D.P., Ritts, W.D., Styles, J.M., Yang, Z., Cohen, W.B., Law, B.E., Thornton, P.E.: A diagnostic carbon flux model to monitor the effects of disturbance and interannual variation in climate on regional NEP, *Tellus B.*, 585, 476–490, 2006.
- Urban, O., Janous, D., Acosta, M., Czerny, R., Markova, I., Navratil, M., Pavelka, M., Pokorny, R., Sprtova, M., Zhang, R., Spunda, V., Grace, J., Marek, M.V.: Ecophysiological controls over the net ecosystem exchange of mountain spruce stand. Comparison of the response in direct vs. diffuse solar radiation, *Global Change Biol.*, 13, 157-168, doi:10.1111/j.1365-2486.2006.01265.x, 2007.
- 695 Van Wijngaarden, W.A., Vincent, L.A.: Trends in relative humidity in Canada from 1953–2003. In 15th Symp. on Global Change and Climate Variations, 2004.
- Veroustraete, F., Sabbe, H., Eerens, H.: Estimation of carbon mass fluxes over Europe using the C-Fix model and Euroflux data, *Remote Sens. Environ.*, 833, 376–399, 2002.
- 700 Vuichard, N., Papale, D.: Filling the gaps in meteorological continuous data measured at FLUXNET sites with ERA-Interim reanalysis, *Earth Syst. Sci. Data*, 7, 157-171, doi:10.5194/essd-7-157-2015, 2015.
- Wang, Z., Skidmore, A.K., Darvishzadeh, R., Wang, T.: Mapping forest canopy nitrogen content by inversion of coupled leaf-canopy radiative transfer models from airborne hyperspectral imagery, *Agric. For. Meteorol.*, 253, 247-260, doi:10.1016/j.agrformet.2018.02.010, 2018.
- 705 Wild, M., Gilgen, H., Roesch, A., Ohmura, A., Long, C.N., Dutton, E.G., Forgan, B., Kallis, A., Russak, V., Tsvetkov, A.: From dimming to brightening: Decadal changes in solar radiation at Earth's surface, *Science*, 308, 847-850, doi:10.1126/science.1103215, 2005.
- Willet, K.M., Dunn, R.J.H., Thorne, P.W., Bell, S., de Podesta, M., Parker, D.E., Jones, P.D., Williams, C.N., Jr.: HadISDH land surface multi-variable humidity and temperature record for climate monitoring, *Climate of the Past*, 10, 1983-2006, doi:10.5194/cp-10-1983-2014, 2014.

- 710 Williams, A.P., Allen, C.D., Macalady, A.K., Griffin, D., Woodhouse, C.A., Meko, D.M., Swetnam, T.W., Rauscher, S.A., Seager, R., Grissino-Mayer, H.D., Dean, J.S., Cook, E.R., Gangodagamage, C., Cai, M., McDowell, N.G.: Temperature as a potent driver of regional forest drought stress and tree mortality, *Nat. Clim. Change*, 3, 292-297, doi:10.1038/nclimate1693, 2013.
- Wu, J., Albert, L.P., Lopes, A.P., Restrepo-Coupe, N., Hayek, M., Wiedemann, K.T., Guan, K., Stark, S.C., Christoffersen, B., Prohaska, N., Tavares, J.V., Marostica, S., Kobayashi, H., Ferreira, M.L., Campos, K.S., da Silva, R., Brando, P.M., Dye, 715 D.G., Huxman, T.E., Huete, A.R., Nelson, B.W., Saleska, S.R.: Leaf development and demography explain photosynthetic seasonality in Amazon evergreen forests, *Science*, 351, 972-976, doi:10.1126/science.aad5068, 2016.
- Wu, J., Guan, K., Hayek, M., Restrepo-Coupe, N., Wiedemann, K.T., Xu, X., Wehr, R., Christoffersen, B.O., Miao, G., da Silva, R., de Araujo, A.C., Oliviera, R.C., Camargo, P.B., Monson, R.K., Huete, A.R., Saleska, S.R.: Partitioning controls on 720 Amazon forest photosynthesis between environmental and biotic factors at hourly to interannual timescales, *Global Change Biol.*, 23, 1240-1257, doi:10.1111/gcb.13509, 2017.
- Xiao, X.M., Zhang, Q.Y., Hollinger, D., Aber, J., Moore, B.: Modeling gross primary production of an evergreen needleleaf forest using MODIS and climate data, *Ecol. Appl.*, 15, 954-969, doi:10.1890/04-0470, 2005.
- Xiao, Z., Liang, S., Wang, J., Xiang, Y., Zhao, X., Song, J.: Long-Time-Series Global Land Surface Satellite Leaf Area Index 725 Product Derived From MODIS and AVHRR Surface Reflectance, *IEEE Trans. Geosci. Remote Sens.*, 54, 5301-5318, doi:10.1109/tgrs.2016.2560522, 2016.
- Xu, B., Li, J., Park, T., Liu, Q., Zeng, Y., Yin, G., Zhao, J., Fan, W., Yang, L., Knyazikhin, Y., Myneni, R.B.: An integrated method for validating long-term leaf area index products using global networks of site-based measurements, *Remote Sens. Environ.*, 209, 134-151, doi:10.1016/j.rse.2018.02.049, 2018.
- 730 Yoder, B.J., Pettigrew-Crosby, R.E.: Predicting nitrogen and chlorophyll content and concentrations from reflectance spectra (400-2500 nm) at leaf and canopy scales, *Remote Sens. Environ.*, 53, 199-211, doi:10.1016/0034-4257(95)00135-n, 1995.
- Yuan, W., Cai, W., Xia, J., Chen, J., Liu, S., Dong, W., Merbold, L., Law, B., Arain, A., Beringer, J., Bernhofer, C., Black, A., Blanken, P.D., Cescatti, A., Chen, Y., Francois, L., Gianelle, D., Janssens, I.A., Jung, M., Kato, T., Kiely, G., Liu, D., Marcolla, B., Montagnani, L., Raschi, A., Rouspard, O., Varlagin, A., Wohlfahrt, G.: Global comparison of light use efficiency 735 models for simulating terrestrial vegetation gross primary production based on the La Thuile database, *Agric. For. Meteorol.*, 192, 108-120, doi:10.1016/j.agrformet.2014.03.007, 2014.
- Yuan, W., Liu, S., Zhou, G., Zhou, G., Tieszen, L.L., Baldocchi, D., Bernhofer, C., Gholz, H., Goldstein, A.H., Goulden, M.L., Hollinger, D.Y., Hu, Y., Law, B.E., Stoy, P.C., Vesala, T., Wofsy, S.C., AmeriFlux, C.: Deriving a light use efficiency model from eddy covariance flux data for predicting daily gross primary production across biomes, *Agric. For. Meteorol.*, 143, 189- 740 207, doi:10.1016/j.agrformet.2006.12.001, 2007.
- Yuan, W., Luo, Y., Li, X., Liu, S., Yu, G., Zhou, T., Bahn, M., Black, A., Desai, A.R., Cescatti, A., Marcolla, B., Jacobs, C., Chen, J., Aurela, M., Bernhofer, C., Gielen, B., Bohrer, G., Cook, D.R., Dragoni, D., Dunn, A.L., Gianelle, D., Gruenwald, T., Ibrom, A., Leclerc, M.Y., Lindroth, A., Liu, H., Marchesini, L.B., Montagnani, L., Pita, G., Rodeghiero, M., Rodrigues, A.,

- 745 Starr, G., Stoy, P.C.: Redefinition and global estimation of basal ecosystem respiration rate, *Global Biogeochem. Cycles*, 2510.1029/2011gb004150, 2011.
- Yuan, W., Liu, S., Yu, G., Bonnefond, J.-M., Chen, J., Davis, K., Desai, A.R., Goldstein, A.H., Gianelle, D., Rossi, F., Suyker, A.E., Verma, S.B.: Global estimates of evapotranspiration and gross primary production based on MODIS and global meteorology data, *Remote Sens. Environ.*, 114, 1416-1431, doi:10.1016/j.rse.2010.01.022, 2010.
- 750 Yuan, W., Zheng, Y., Piao, S., Ciais, P., Lombardozzi, D., Wang, Y., Ryu, Y., Chen, G., Dong, W., Hu, Z., Jain, A.K., Jiang, C., Kato, E., Li, S., Lienert, S., Liu, S., Nabel, J.E.M.S., Qin, Z., Quine, T., Sitch, S., Smith, W.K., Wang, F., Wu, C., Xiao, Z., Yang, S.: Increased atmospheric vapor pressure deficit reduces global vegetation growth, *Science Advances*, 5, eaax1396, 2019.
- Zhang, H. Q., Pak, B., Wang, Y. P., Zhou, X. Y., Zhang, Y. Q., and Zhang, L.: Evaluating Surface Water Cycle Simulated by the Australian Community Land Surface Model (CABLE) across Different Spatial and Temporal Domains, *J. of Hydrometeorol.*, 14, 1119–1138, 2013.
- 755 Zhang, Y., Xiao, X., Wu, X., Zhou, S., Zhang, G., Qin, Y., Dong, J.: Data Descriptor: A global moderate resolution dataset of gross primary production of vegetation for 2000-2016, *Scientific Data*, 410.1038/sdata.2017.165, 2017.
- Zhao, M., Running, S.W.: Drought-Induced Reduction in Global Terrestrial Net Primary Production from 2000 Through 2009, *Science*, 329, 940-943, doi:10.1126/science.1192666, 2010.
- 760 Zheng, Y., Shen, R.; Wang, Y., Li, X., Liu, S., Liang, S., Chen, Jing M., Ju, W., Zhang, L., Yuan, W.: Improved estimate of global gross primary production for reproducing its long-term variation, 1982-2017. figshare. Dataset. doi:10.6084/m9.figshare.8942336, 2019.
- Zheng, Y., Zhang, L., Xiao, J., Yuan, W., Yan, M., Li, T., Zhang, Z.: Sources of uncertainty in gross primary productivity simulated by light use efficiency models: Model structure, parameters, input data, and spatial resolution, *Agric. For. Meteorol.*, 765 263, 242-257, doi:10.1016/j.agrformet.2018.08.003, 2018.
- Zhou, S., Williams, A. P., Berg, A. M., Cook, B. I., Zhang, Y., Hagemann, S., Lorenz, R., Seneviratne, S. I., and Gentine, P.: Land-atmosphere feedbacks exacerbate concurrent soil drought and atmospheric aridity, *Proc. Natl. Acad. Sci. U.S.A.*, 116, 18848-18853, 2019a.
- Zhou, S., Zhang, Y., Williams, A. P., and Gentine, P.: Projected increases in intensity, frequency, and terrestrial carbon costs of compound drought and aridity events, *Science Advances*, 5, eaau5740, 2019b.
- 770 Zhu, Z., Piao, S., Myneni, R.B., Huang, M., Zeng, Z., Canadell, J.G., Ciais, P., Sitch, S., Friedlingstein, P., Arneeth, A., Cao, C., Cheng, L., Kato, E., Koven, C., Li, Y., Lian, X., Liu, Y., Liu, R., Mao, J., Pan, Y., Peng, S., Penuelas, J., Poulter, B., Pugh, T.A.M., Stocker, B.D., Viovy, N., Wang, X., Wang, Y., Xiao, Z., Yang, H., Zaehle, S., Zeng, N.: Greening of the Earth and its drivers, *Nat. Clim. Change*, 6, 791-796, doi:10.1038/nclimate3004, 2016.

775

Tables

Table 1: Information on the eddy covariance (EC) sites used in this study.

Site Name	Latitude	Longitude	Vegetation Type	Study Period
*DE-Kli	50.89°N	13.52°E	CRO	2004-2012
DE-RuS	50.87°N	6.45°E	CRO	2011-2012
FI-Jok	60.90°N	23.51°E	CRO	2001-2003
*FR-Gri	48.84°N	1.95°E	CRO	2005-2012
*US-ARM	36.61°N	97.49°W	CRO	2003-2012
*US-Ne1	41.16°N	96.47°W	CRO	2001-2012
*US-Ne2	41.16°N	96.47°W	CRO	2001-2012
*US-Ne3	41.17°N	96.43°W	CRO	2001-2012
CA-TPD	42.64°N	80.56°W	DBF	2012
*DE-Hai	51.08°N	10.45°E	DBF	2000-2012
*DK-Sor	55.49°N	11.64°E	DBF	2001-2012
*FR-Fon	48.48°N	2.78°E	DBF	2005-2012
IT-PT1	45.20°N	9.06°E	DBF	2002-2004
*IT-Ro2	42.39°N	11.92°E	DBF	2002-2008; 2010-2012
JP-MBF	44.39°N	142.32°E	DBF	2004-2005
*US-Ha1	42.54°N	72.17°W	DBF	1992-2012
*US-MMS	39.32°N	86.41°W	DBF	1999-2012
*US-Oho	41.55°N	83.84°W	DBF	2004-2012
*US-UMB	45.56°N	84.71°W	DBF	2000-2012
*US-UMd	45.56°N	84.70°W	DBF	2008-2012
*US-WCr	45.81°N	90.08°W	DBF	1999-2006; 2011-2012
*BR-Sa1	2.86°S	54.96°W	EBF	2002-2005; 2008-2011
BR-Sa3	3.02°S	54.97°W	EBF	2001-2003
CN-Din	23.17°N	112.54°E	EBF	2003-2005
*FR-Pue	43.74°N	3.60°E	EBF	2000-2012
*GF-Guy	5.28°N	52.92°W	EBF	2004-2012
*MY-PSO	2.97°N	102.31°E	EBF	2003-2009
CA-NS1	55.88°N	98.48°W	ENF	2002-2005
*CA-NS2	55.91°N	98.52°W	ENF	2001-2005
CA-NS3	55.91°N	98.38°W	ENF	2002-2005
CA-NS4	55.91°N	98.38°W	ENF	2003-2005
*CA-NS5	55.86°N	98.49°W	ENF	2001-2005

*CA-Qfo	49.69°N	74.34°W	ENF	2003-2010
CA-SF1	54.49°N	105.82°W	ENF	2003-2006
*CA-SF2	54.25°N	105.88°W	ENF	2001-2005
*CA-TP1	42.66°N	80.56°W	ENF	2003-2012
*CA-TP2	42.77°N	80.46°W	ENF	2003-2007
*CA-TP3	42.71°N	80.35°W	ENF	2003-2012
CN-Qia	26.74°N	115.06°E	ENF	2003-2005
*CZ-BK1	49.50°N	18.54°E	ENF	2004-2012
DE-Lkb	49.10°N	13.30°E	ENF	2009-2012
*DE-Obe	50.78°N	13.72°E	ENF	2008-2012
*DE-Tha	50.96°N	13.57°E	ENF	1996-2012
*FI-Hyy	61.85°N	24.30°E	ENF	1996-2012
IT-La2	45.95°N	11.29°E	ENF	2001
*IT-Lav	45.96°N	11.28°E	ENF	2003-2012
*IT-Ren	46.59°N	11.43°E	ENF	1999-2012
*IT-SRo	43.73°N	10.28°E	ENF	2001-2012
*NL-Loo	52.17°N	5.74°E	ENF	1996-2012
*RU-Fyo	56.46°N	32.92°E	ENF	1998-2012
*US-Blo	38.90°N	120.63°W	ENF	1997-2007
*US-Me2	44.45°N	121.56°W	ENF	2002-2012
US-Me6	44.32°N	121.61°W	ENF	2011-2012
*US-NR1	40.03°N	105.55°W	ENF	1999-2012
*CH-Cha	47.21°N	8.41°E	GRA	2006-2008; 2010-2012
*CH-Fru	47.12°N	8.54°E	GRA	2006-2008; 2010-2012
*CH-Oe1	47.29°N	7.73°E	GRA	2002-2008
CN-Cng	44.59°N	123.51°E	GRA	2007-2010
CN-Du2	42.05°N	116.28°E	GRA	2007-2008
CN-HaM	37.37°N	101.18°E	GRA	2002-2003
*CZ-BK2	49.49°N	18.54°E	GRA	2006-2011
*NL-Hor	52.24°N	5.07°E	GRA	2004-2011
RU-Ha1	54.73°N	90.00°E	GRA	2002-2004
US-AR1	36.43°N	99.42°W	GRA	2009-2012
US-AR2	36.64°N	99.60°W	GRA	2009-2012
*US-Goo	34.25°N	89.87°W	GRA	2002-2006
*US-IB2	41.84°N	88.24°W	GRA	2005; 2007-2011
*BE-Bra	51.31°N	4.52°E	MF	1999-2002; 2004-2012
*BE-Vie	50.31°N	6.00°E	MF	1997-2012

*CA-Gro	48.22°N	82.16°W	MF	2004-2012
CN-Cha	42.40°N	128.10°E	MF	2003-2005
JP-SMF	35.26°N	137.08°E	MF	2003-2006
*US-PFa	45.95°N	90.27°W	MF	1996-2012
*US-Syv	46.24°N	89.35°W	MF	2001-2006; 2012
AU-Ade	13.08°S	131.12°E	SAV	2007-2009
AU-Cpr	34.00°S	140.59°E	SAV	2011-2012
*AU-DaS	14.16°S	131.39°E	SAV	2008-2012
AU-Dry	15.26°S	132.37°E	SAV	2009-2012
AU-RDF	14.56°S	132.48°E	SAV	2011-2012
SD-Dem	13.28°N	30.48°E	SAV	2007-2009
*US-Ton	38.43°N	120.97°W	SAV	2001-2012
ZA-Kru	25.02°S	31.50°E	SAV	2009-2012
CA-NS6	55.92°N	98.96°W	SRH	2002-2005
CA-NS7	56.64°N	99.95°W	SRH	2003-2005
*CA-SF3	54.09°N	106.01°W	SRH	2002-2006
ES-LgS	37.10°N	2.97°W	SRH	2007-2009
US-KS2	28.61°N	80.67°W	SRH	2003-2006
CN-Ha2	37.61°N	101.33°E	WET	2003-2005
DE-Akm	53.87°N	13.68°E	WET	2010-2012
DE-SfN	47.81°N	11.33°E	WET	2012
DE-Spw	51.89°N	14.03°E	WET	2010-2012
RU-Che	68.61°N	161.34°E	WET	2002-2004
US-Ivo	68.49°N	155.75°W	WET	2004-2007
*US-Los	46.08°N	89.98°W	WET	2001-2008; 2010
US-WPT	41.46°N	83.00°W	WET	2011-2012

* indicates the site used to investigate the interannual variations in GPP with observations greater than 5-years.

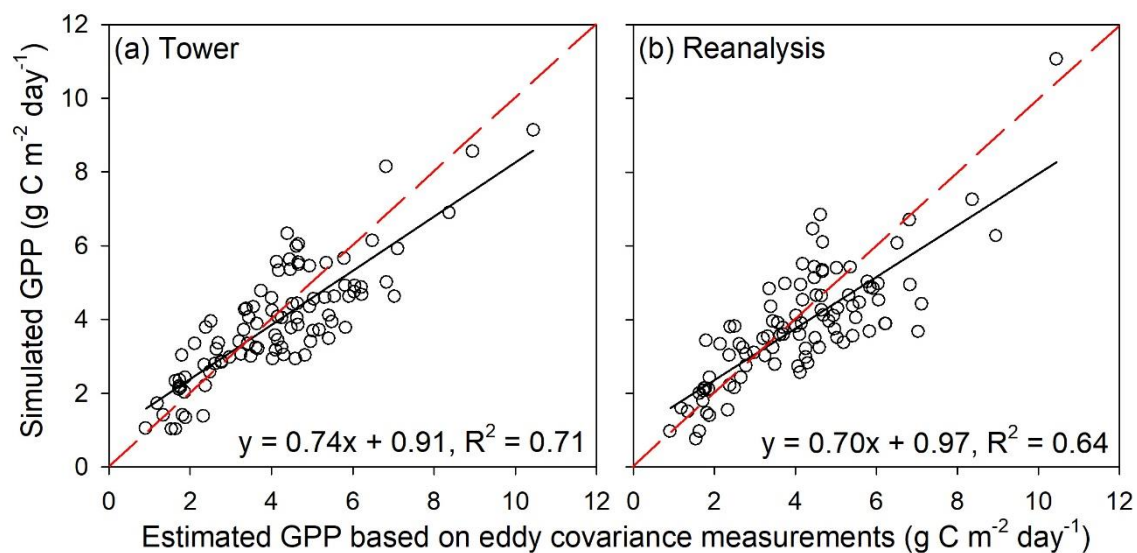
Table 2: Input datasets used to drive the revised EC-LUE model.

Variable	Dataset/provider	Source
Air temperature	MERRA2	https://gmao.gsfc.nasa.gov/reanalysis/MERRA-2/
Dew point temperature	MERRA2	https://gmao.gsfc.nasa.gov/reanalysis/MERRA-2/
Direct PAR	MERRA2	https://gmao.gsfc.nasa.gov/reanalysis/MERRA-2/
Diffuse PAR	MERRA2	https://gmao.gsfc.nasa.gov/reanalysis/MERRA-2/
LAI	GLASS	http://www.glass.umd.edu/Download.html
Landcover map	MCD12Q1	https://lpdaac.usgs.gov/products/mcd12q1v006/
C4 crop percentage	ISLSCP II C4 Vegetation Percentage	https://doi.org/10.3334/ORNLDAAAC/932
CO ₂ concentration	NOAA's Earth System Research Laboratory	www.esrl.noaa.gov/gmd/ccgg/trends/

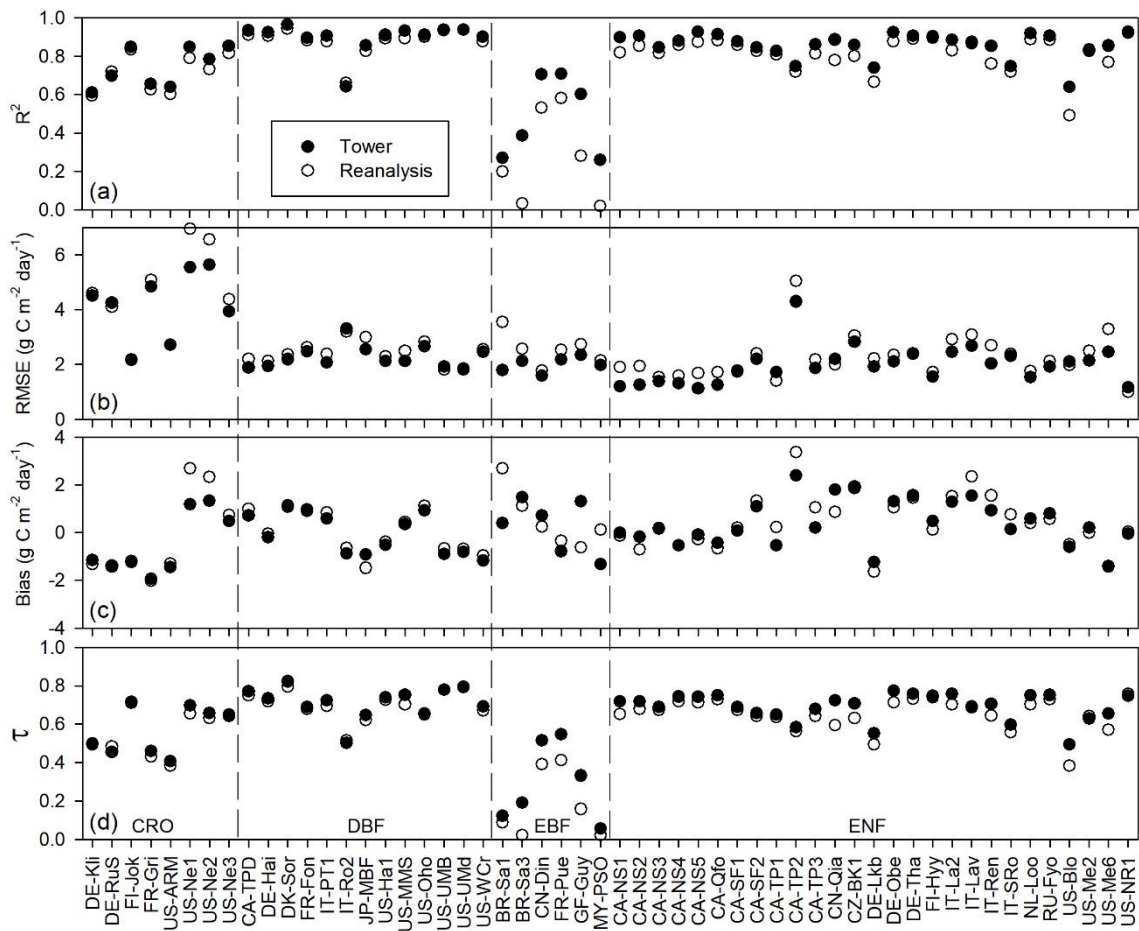
Table 3: Optimized parameters (ϵ_{msu} , ϵ_{msh} , ϕ , and VPD_0) of the revised EC-LUE model for different vegetation types.

Vegetation Types	DBF	ENF	EBF	MF	GRA	CRO-C3	CRO-C4	SAV	SHR	WET
ϵ_{msu} (g C MJ ⁻¹)	1.28 ± 0.36	1.72 ± 0.42	1.67 ± 0.85	1.38 ± 0.21	1.16 ± 0.15	1.25 ± 0.42	2.46 ± 0.78	2.24 ± 0.68	1.21 ± 0.25	1.34 ± 0.26
ϵ_{msh} (g C MJ ⁻¹)	3.59 ± 0.66	3.87 ± 0.58	4.35 ± 0.72	3.29 ± 0.63	1.91 ± 0.46	2.46 ± 0.52	5.64 ± 1.02	4.26 ± 0.95	2.71 ± 0.52	2.62 ± 0.49
ϕ (ppm)	32 ± 8.25	25 ± 7.59	20 ± 6.36	49 ± 11.25	57 ± 11.85	43 ± 9.56	54 ± 15.36	54 ± 12.23	34 ± 7.59	36 ± 10.32
VPD_0 (k Pa)	1.15 ± 0.25	1.34 ± 0.26	0.57 ± 0.15	0.62 ± 0.14	1.69 ± 0.35	1.02 ± 0.19	1.53 ± 0.31	1.65 ± 0.26	1.34 ± 0.21	0.62 ± 0.12

Figures



790 **Figure 1: Comparisons between annual mean GPP estimated from EC towers and annual mean GPP simulated by the revised EC-LUE model. The modeled GPP were simulated using (a) tower-derived meteorology and (b) global reanalysis meteorology. The black lines are the regression lines, and the red dash lines are the 1:1 lines. The insert equations are the regression equations derived from all the sites.**

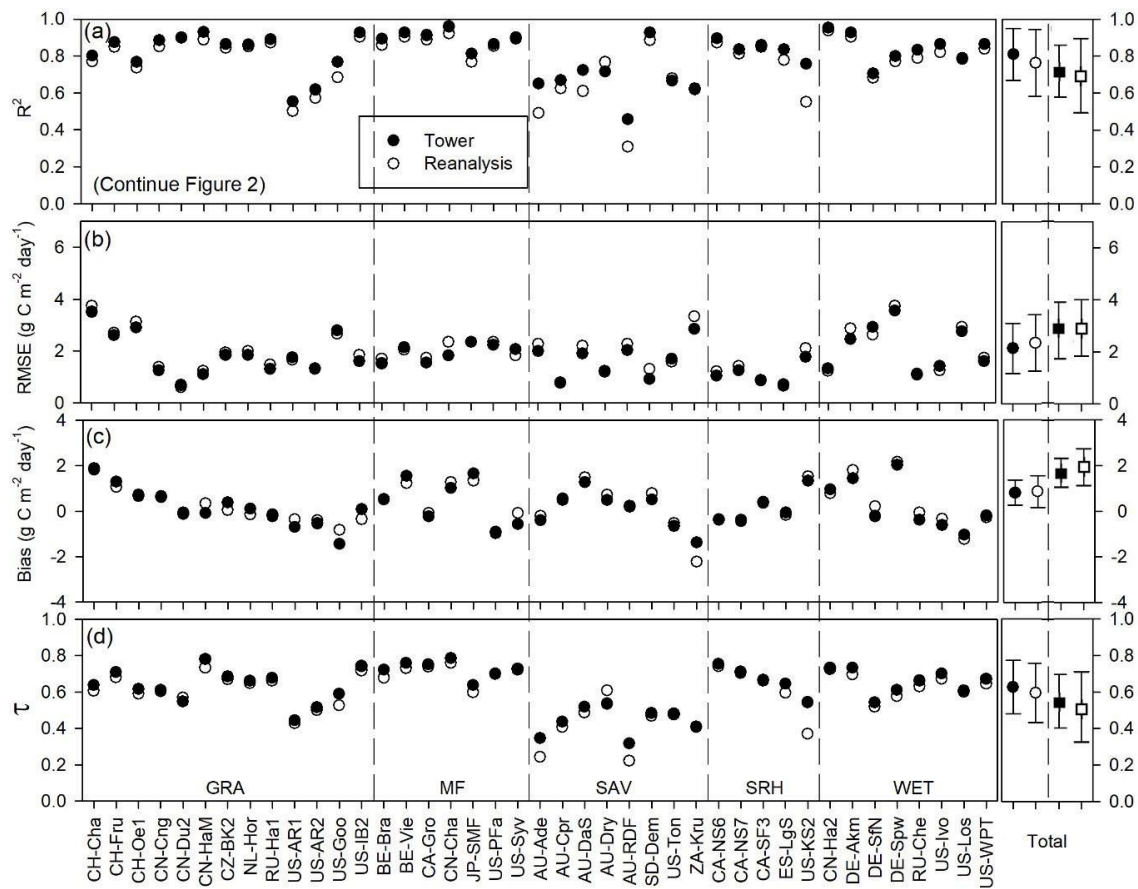


795

Figure 2: Comparisons of 8-day mean GPP between the model simulated GPP and tower estimated GPP. Solid and open dots indicate the GPP simulations of the revised EC-LUE model derived from tower-derived meteorology data and meteorological reanalysis dataset, respectively; solid and open squares indicate the GPP simulations of the original EC-LUE model derived from tower-derived meteorology data and meteorological reanalysis dataset, respectively.

800

Figure 2 (continue)



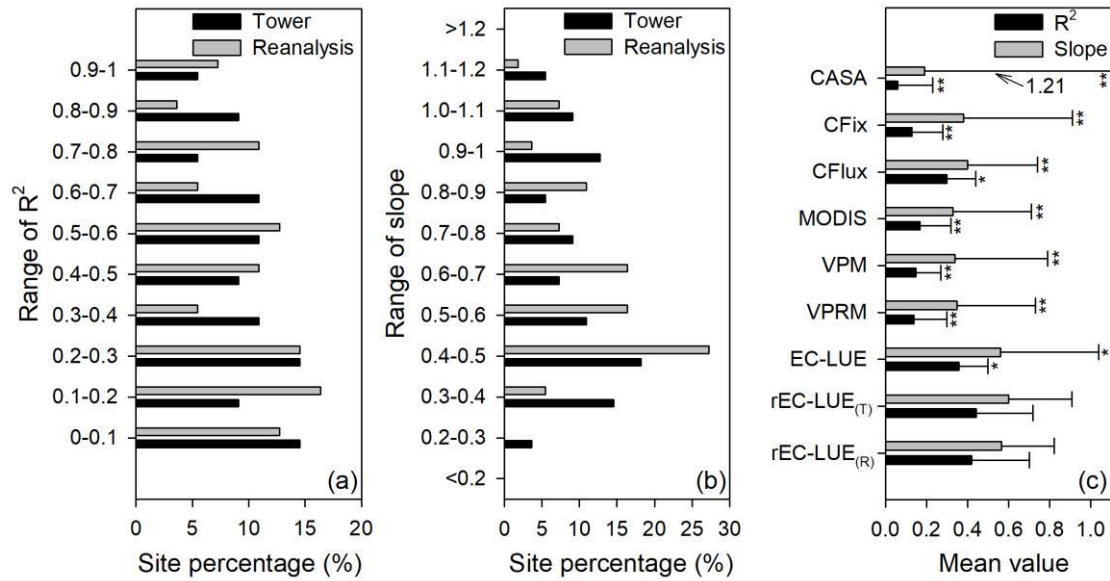
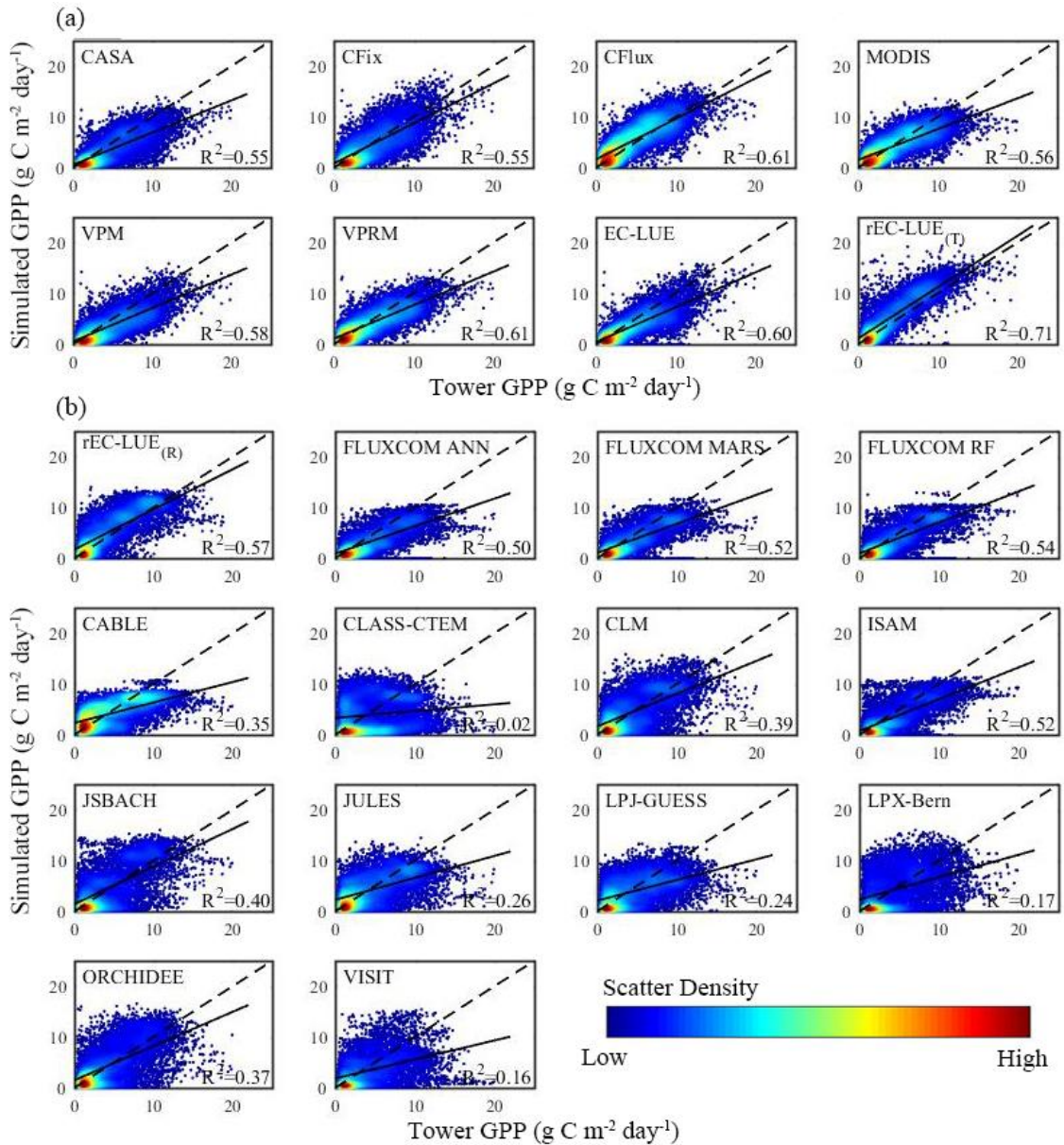


Figure 3: Site percentage of (a) correlation coefficients (R^2), and (b) regression slopes between the model simulated and tower-based interannual variabilities in GPP. (c) Averaged values (error bars represent the standard deviations) of R^2 and slope for various LUE models. rEC-LUE_(T) and rEC-LUE_(R) indicate the revised EC-LUE models derived from tower-derived meteorology data and meteorological reanalysis dataset. The R^2 and slopes of the other seven LUE models (i.e., EC-LUE, VPRM, VPM, MODIS, CFlux, CFix, and CASA) in the figure were obtained from the study by Yuan et al. (2014). ** and * indicate a significant difference in statistic variables (R^2 and slope) between the rEC-LUE_(T) and other LUE models (i.e., rEC-LUE_(T) and other seven LUE models) at p -value < 0.01 and p -value < 0.05, respectively.

810



815

Figure 4: Comparisons between estimated GPP based on EC measurements and GPP simulations in growing season (defined as temperature larger than 0°C) by the various models (including LUE models, machine learning models, and process-based models in TRENDY) at monthly scale. The comparison of GPP simulations were simulated using (a) tower-derived meteorology data and (b) global reanalysis meteorology data, respectively (see method 2.4). rEC-LUE_(T) and rEC-LUE_(R) indicate the simulations of the revised EC-LUE model derived from tower-derived meteorology data and global reanalysis meteorology data, respectively.

820

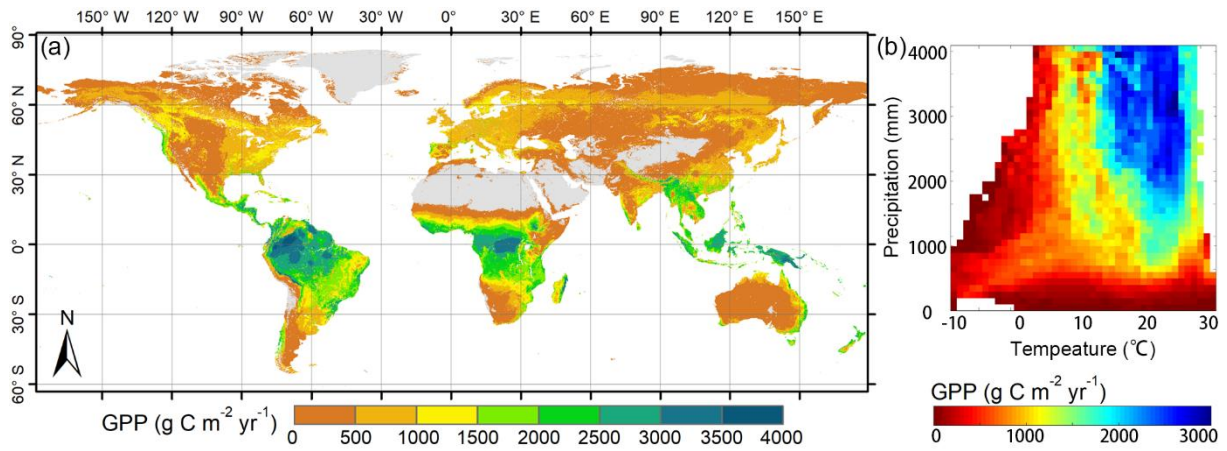


Figure 5: Spatial pattern of global GPP simulated by the revised EC-LUE model during 1982–2017: (a) averaged annual GPP, (b) averaged annual GPP at different temperature and precipitation gradients.

825

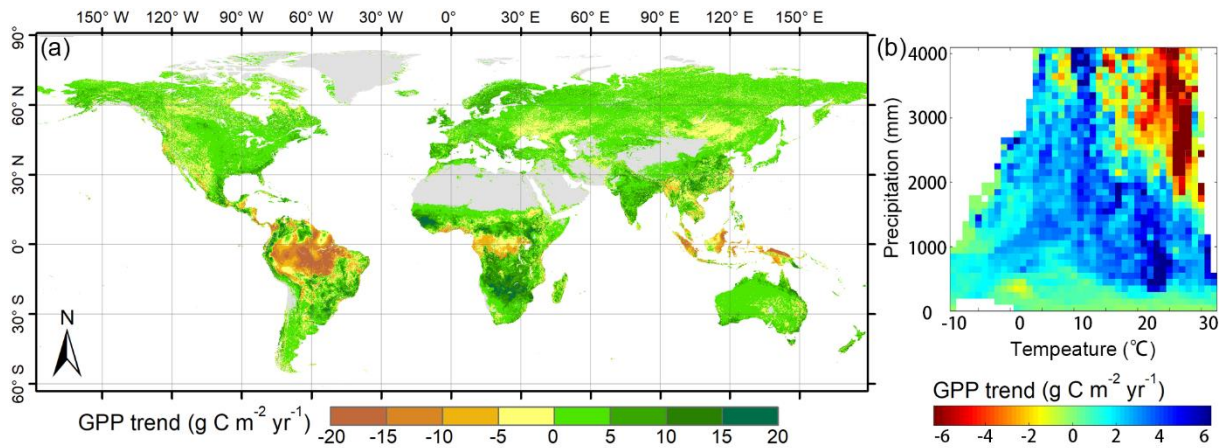
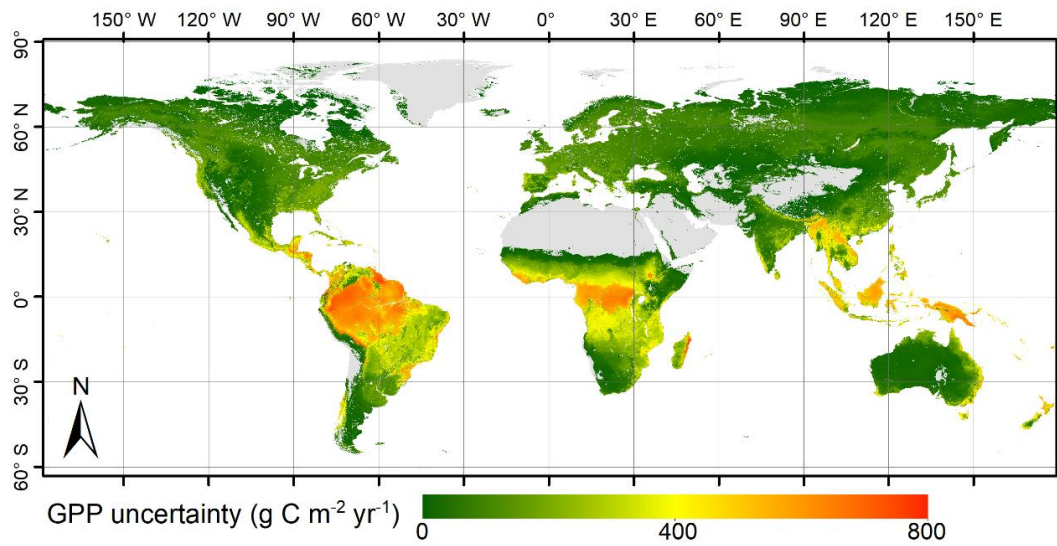
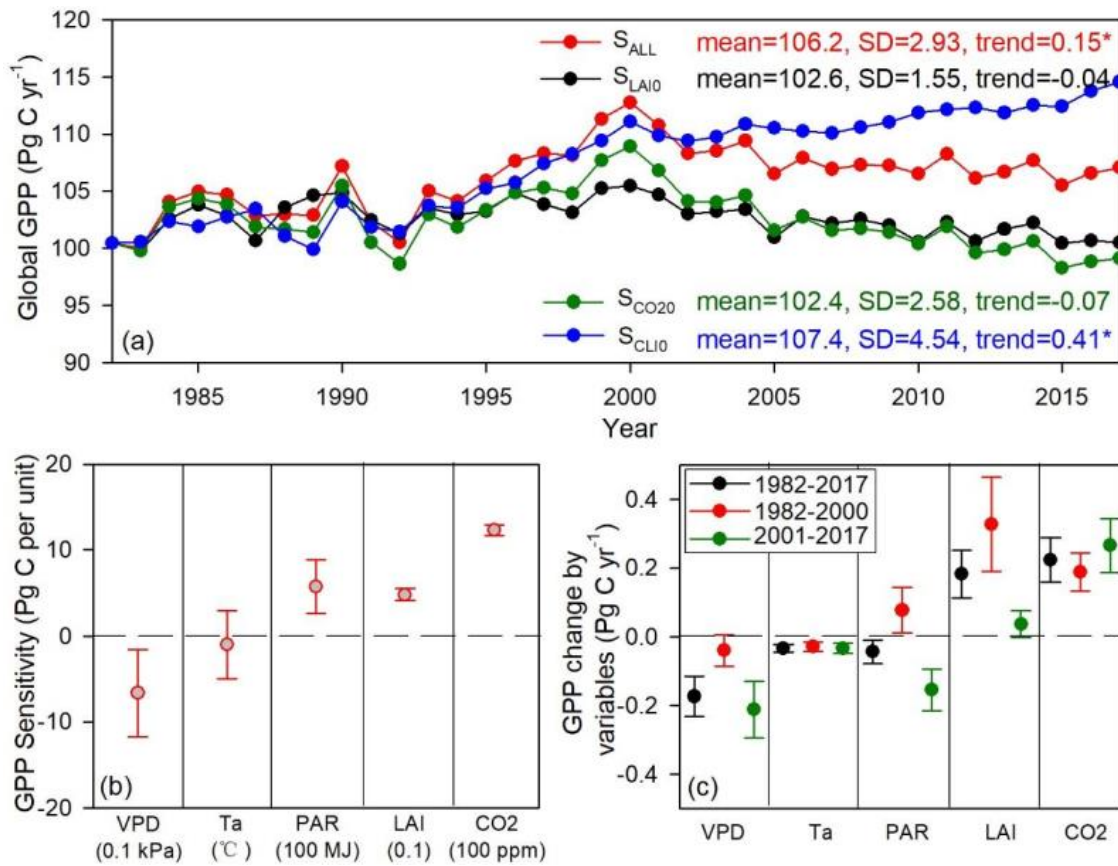


Figure 6: Spatial pattern of global GPP trend simulated by the revised EC-LUE models during 1982–2017: (a) trend of annual GPP, (b) trend of annual GPP at different temperature and precipitation gradients.

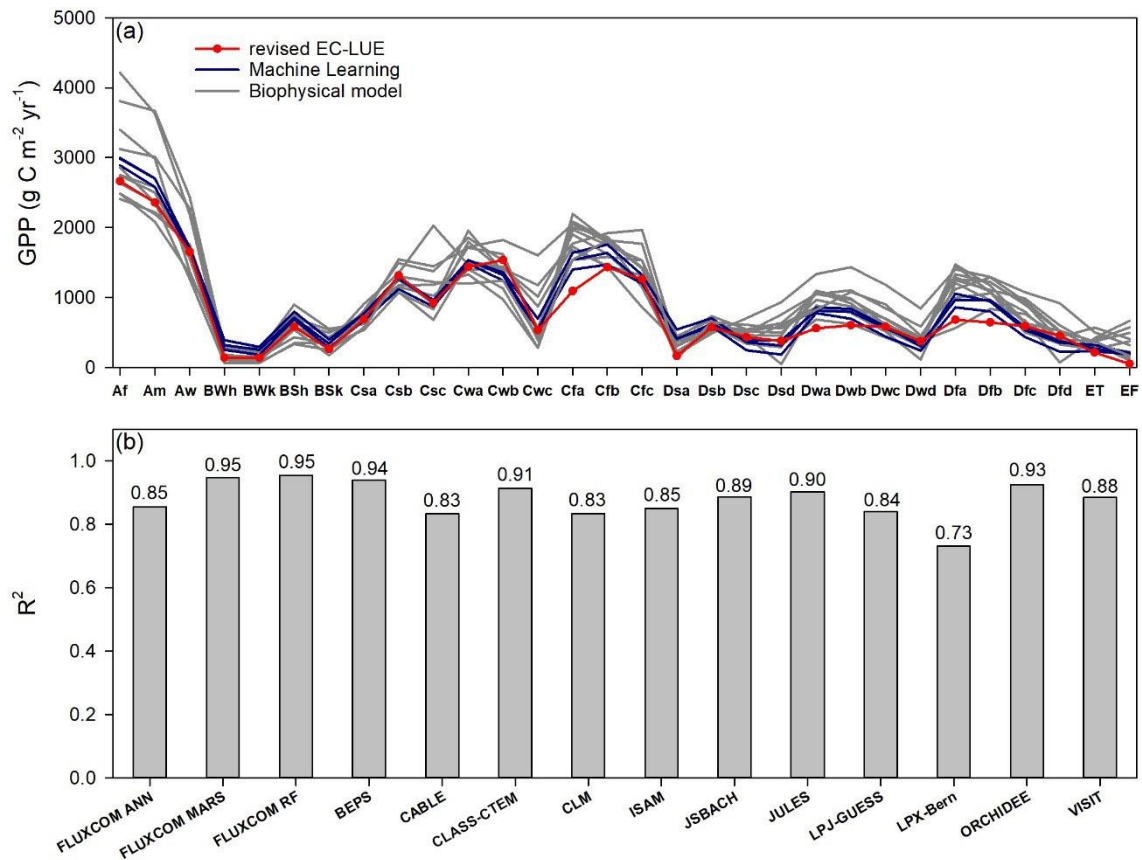


830

Figure 7: Spatial pattern of the uncertainty in global GPP simulated by the revised EC-LUE model.



835 **Figure 8: Long-term changes in global GPP and the environmental regulations: (a) Global summed GPP derived from the four experimental simulations in section 2.5, (b) GPP sensitivity to climate variables (i.e., VPD, Ta, and PAR), LAI, and atmospheric CO₂, (c) contributions of climate variables (i.e., VPD, Ta, and PAR), LAI, and atmospheric CO₂ to GPP changes over 1982–2017, 1982–2000, and 2001–2017. * indicates the significant level at p -value<0.05.**



840 **Figure 9: Comparisons of long-term (1982 to 2010s) averaged GPP between the revised EC-LUE model and other models across**
bioclimatic zones in the Köppen-Geiger climate classification map (Beck et al., 2018). (a) the regional averaged value (b) correlation
coefficients (R^2) of GPP across all the bioclimatic zones between the revised EC-LUE model and other models. These models
including machine learning models (FLUXCOM ANN, FLUXCOM MARS, FLUXCOM RF; Jung et al., 2017), biophysical models
BEPS (Ju et al., 2006; Liu et al., 2018), and ten biophysical models in TRENDY (CABLE, CLASS-CTEM, CLM, ISAM, JSBACH,
845 **JULES, LPJ-GUESS, LPX-Bern, ORCHIDEE, and VISIT). The abbreviations for the bioclimatic zones are as follows: Af, tropical,**
rainforest; Am, tropical, monsoon; Aw, tropical, savannah; BWh, arid, desert, hot; BWk, arid, desert, cold; BSh, arid, steppe, hot;
BSk, arid, steppe, cold; Csa, temperate, dry summer, hot summer; Csb, temperate, dry summer, warm summer; Csc, temperate,
850 **dry summer, cold summer; Cwa, temperate, dry winter, hot summer; Cwb, temperate, dry winter, warm summer; Cwc, temperate,**
dry winter, cold summer; Cfa, temperate, no dry season, hot summer; Cfb temperate, no dry season, warm summer; Cfc, temperate,
no dry season, cold summer; Dsa, cold, dry summer, hot summer; Dsb, cold, dry summer, warm summer; Dsc, cold, dry summer,
cold summer; Dsd, cold, dry summer, very cold winter; Dwa, cold, dry winter, hot summer; Dwb, cold, dry winter, warm summer;
Dwc, cold, dry winter, cold summer; Dwd, cold, dry winter, very cold winter; Dfa, cold, no dry season, hot summer; Dfb, cold, no
dry season, warm summer; Dfc, cold, no dry season, cold summer; Dfd, cold, no dry season, very cold winter; ET, polar, tundra;
EF, polar, frost.

855

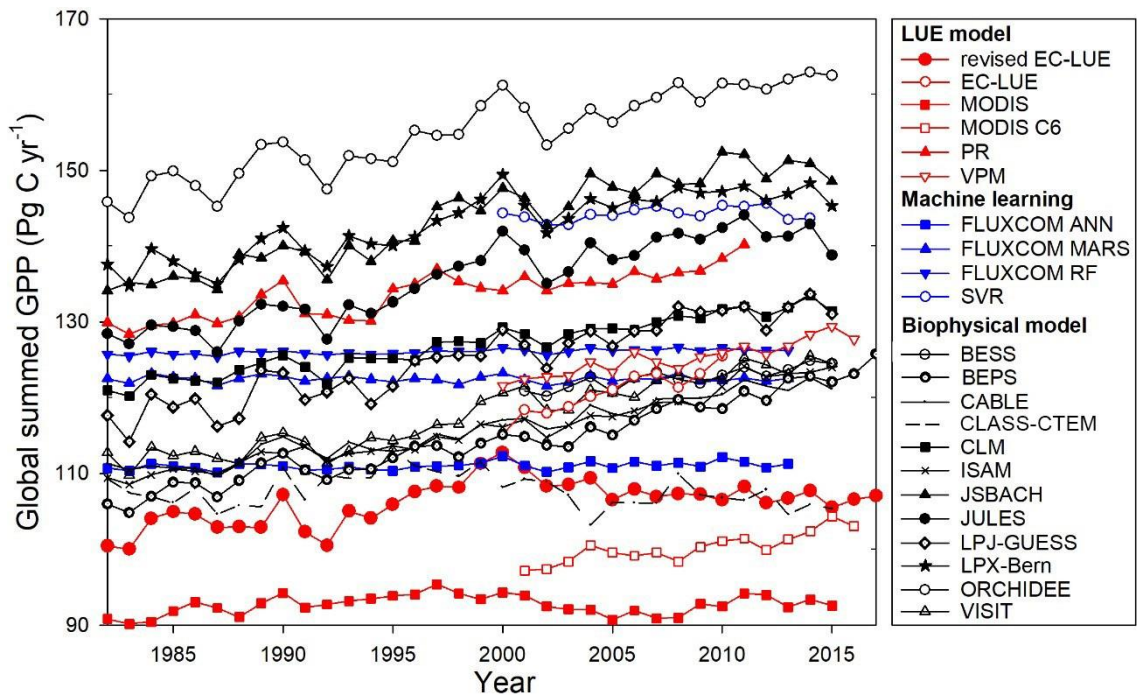
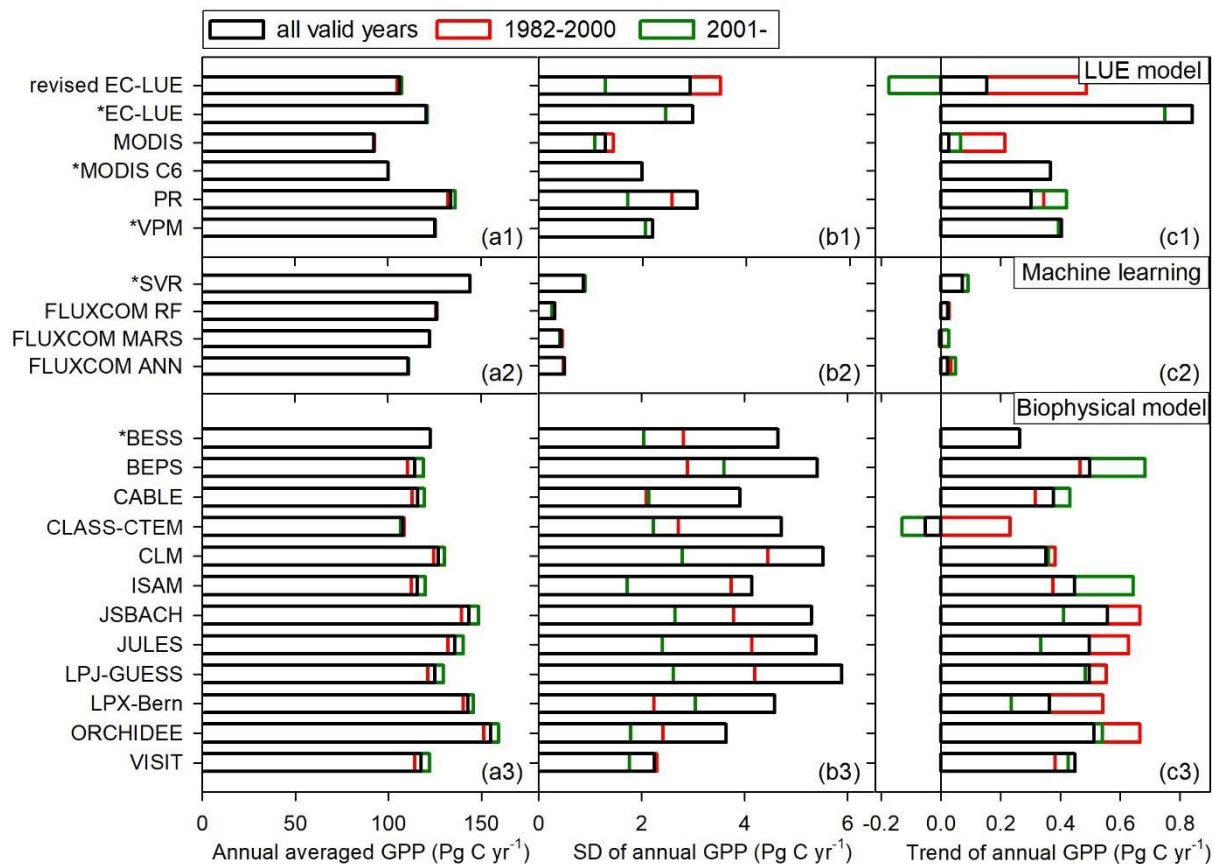


Figure 10: Comparisons of annual global summed GPP estimates from various models. The datasets or model algorithms were obtained from: EC-LUE (Cai et al., 2014), MODIS (Smith et al., 2016), MOD17 C6 (Running et al., 2004), PR (Keenan et al., 2016), VPM (Zhang et al., 2017), FLUXCOM (Jung et al., 2017), SVR (Kondo et al., 2015), BESS (Jiang and Ryu, 2016), BEPS (Ju et al., 2006; Liu et al., 2018), and models in TRENDY (CABLE, CLASS-CTEM, CLM, ISAM, JSBACH, JULES, LPJ-GUESS, LPX-Bern, ORCHIDEE, and VISIT).

860



865 **Figure 11: Comparison of (a1)–(a3) averaged annual GPP, (b1)–(b3) interannual variability in annual GPP represented by standard deviation (SD), and (c1)–(c3) annual GPP trend among different GPP datasets or models. The references of these models are the same as in Figure 9. * indicates that the valid period of the dataset begins from 2000 or 2001.**